



Elevated Hoxb5b Expands Vagal Neural Crest Pool and Blocks Enteric Neuronal Development in Zebrafish

Aubrey G. A. Howard IV¹, Aaron C. Nguyen¹, Joshua Tworig², Priya Ravisankar^{3,4}, Eileen W. Singleton¹, Can Li², Grayson Kotzur¹, Joshua S. Waxman³ and Rosa A. Uribe^{1*}

¹BioSciences Department, Rice University, Houston, TX, United States, ²Division of Biology and Biological Engineering, California Institute of Technology, Pasadena, CA, United States, ³Molecular Cardiovascular Biology Division, Cincinnati Children's Hospital Medical Center and Department of Pediatrics, University of Cincinnati College of Medicine, Cincinnati, OH, United States, ⁴Allen Institute of Immunology, Seattle, WA, United States

OPEN ACCESS

Edited by:

Ernesto Sánchez-Herrero,
Spanish National Research Council
(CSIC), Spain

Reviewed by:

Sally Ann Moody,
George Washington University,
United States
Maria Elena De Bellard,
California State University, Northridge,
United States

*Correspondence:

Rosa A. Uribe
rosa.uribe@rice.edu

Specialty section:

This article was submitted to
Morphogenesis and Patterning,
a section of the journal
Frontiers in Cell and Developmental
Biology

Received: 27 October 2021

Accepted: 13 December 2021

Published: 31 January 2022

Citation:

Howard AGA, Nguyen AC, Tworig J,
Ravisankar P, Singleton EW, Li C,
Kotzur G, Waxman JS and Uribe RA
(2022) Elevated Hoxb5b Expands
Vagal Neural Crest Pool and Blocks
Enteric Neuronal Development
in Zebrafish.
Front. Cell Dev. Biol. 9:803370.
doi: 10.3389/fcell.2021.803370

Neural crest cells (NCCs) are a migratory, transient, and multipotent stem cell population essential to vertebrate embryonic development, contributing to numerous cell lineages in the adult organism. While great strides have been made in elucidating molecular and cellular events that drive NCC specification, comprehensive knowledge of the genetic factors that orchestrate NCC developmental programs is still far from complete. We discovered that elevated Hoxb5b levels promoted an expansion of zebrafish NCCs, which persisted throughout multiple stages of development. Correspondingly, elevated Hoxb5b also specifically expanded expression domains of the vagal NCC markers *foxd3* and *phox2bb*. Increases in NCCs were most apparent after pulsed ectopic Hoxb5b expression at early developmental stages, rather than later during differentiation stages, as determined using a novel transgenic zebrafish line. The increase in vagal NCCs early in development led to supernumerary Phox2b⁺ enteric neural progenitors, while leaving many other NCC-derived tissues without an overt phenotype. Surprisingly, these NCC-derived enteric progenitors failed to expand properly into sufficient quantities of enterically fated neurons and stalled in the gut tissue. These results suggest that while Hoxb5b participates in vagal NCC development as a driver of progenitor expansion, the supernumerary, ectopically localized NCC fail to initiate expansion programs in timely fashion in the gut. All together, these data point to a model in which Hoxb5b regulates NCCs both in a tissue specific and temporally restricted manner.

Keywords: neural crest, hox, zebrafish, enteric neuron, differentiation

INTRODUCTION

As an embryonic stem cell population in vertebrates, neural crest cells (NCCs) are renowned for their remarkable migratory capacity, as well as their multipotency. Born from the dorsal neural tube, NCCs migrate along stereotypic routes throughout the early embryo and give rise to a wide range of diverse tissue lineages, such as craniofacial skeleton, portions of the peripheral nervous system, and pigment cells (Rocha et al., 2020). NCCs exhibit regional potential along the anteroposterior (AP) neuraxis such that they may be divided into four general populations: cranial, vagal, trunk, and sacral (Le Douarin, 1982; Le Douarin and Kalcheim, 1999). Each of these populations give rise to numerous discrete lineages, for example, cranial NCC largely give rise to cell lineages in the head. Particularly of

interest are vagal NCCs, which contribute to several tissues, such as the cardiac outflow tract and nearly all of the enteric nervous system (ENS) (Tang et al., 2021) within the gut, and have been less well characterized than other populations (Hutchins et al., 2018). While the driving genetic factors which regulate the general pattern of NCC developmental trajectories have been well described (Simoes-Costa and Bronner, 2016; Martik and Bronner, 2017), we still have an incomplete understanding of what genes function in context of vagal NCC development and their subsequent differentiation.

Coincident with the anterior to posterior rise of NCC is the expression of Hox genes, a strongly conserved family of genes encoding for transcription factors most notable for their canonical role in body axis patterning (Amores et al., 1998; Pearson et al., 2005). Among their many roles, Hox transcription factors are known to play essential roles in establishing discrete partitions within the hindbrain, directing limb formation, regulating cardiac cell number, and guiding neural circuit formation within a variety of tissue contexts (Rancourt et al., 1995; Waxman et al., 2008; Minguillon et al., 2012; Breau et al., 2013; Di Bonito et al., 2013; Barsh et al., 2017). Organized in tight clusters in the genome, known as paralogy groups, Hox genes are labeled A–D to designate a particular chromosomal cluster, as well as by number, which represents the gene's chromosomal position within a particular cluster, ranging from 1–13 (Kudoh et al., 2001). Furthermore, not only are the Hox peptide sequences conserved between species, synteny of the Hox clusters is highly conserved (Santini et al., 2003). The role of Hox genes among vertebrates is also strongly conserved in their function, even among teleost fishes who have undergone a genome duplication during their evolutionary history (Amores et al., 1998; Parker et al., 2019). Each Hox gene is expressed along the anterior-posterior axis in nested domains collinear with their position in the chromosome, where they undergo complex regulatory interaction to establish discrete expression domains (Zhu et al., 2017). As such, earlier numbered Hox factors are commonly expressed within the cephalic tissues, while later numbered Hox factors are expressed more distally.

Within the context of cranial NCCs, Hox transcription factors have been shown to drive a number of NCC phenotypes. Overexpression of Hox factors in chicken, such as *Hoxa2*, *Hoxa3*, and *Hoxb4*, produces a variety of overlapping ablations of NCC-derived craniofacial skeleton (Creuzet et al., 2002). Similarly, the NCC-derived hyoid bones and presumptive thymic mesenchyme were greatly reduced or ablated in mice homozygous for single knockout for *Hoxa-3*, or double knockout of *Hoxa-3* and *Hoxd-3*, while also causing homeotic transformations of other structures throughout the animal (Condie and Capecchi, 1993, 1994). In addition to affecting formation of terminally differentiated craniofacial structures, earlier phases of NCC migration into pharyngeal arches and onset emigration of NCC from the neural tube are also acutely sensitive to changes in anterior Hox expression (Gouti et al., 2011; Parker et al., 2018). While the role of Hox transcription factors is less well characterized in posterior populations of NCC, vagal NCC in mice fail to colonize the

gut following overexpression of *Hoxa-4*, which is endemic to the gut nervous network (Wolgemuth et al., 1989; Tennyson et al., 1993). The failure to form a complete enteric nervous system results in megacolon, a phenotype associated with human disease (Nagy and Goldstein, 2017). Overall, while we have learned much regarding Hox genes in the cranial NCC, the roles Hox transcription factors play within vagal and other posterior NCC populations requires further investigation.

One posterior Hox factor that has been implicated in vagal NCC development is Hoxb5. In mice, dominant negative abrogation of embryonic Hoxb5 activity alters vagal and trunk NCC development, with reduced NCCs observed en route to and along gut tissue, as well as decreased numbers of melanoblasts throughout the body (Lui et al., 2008; Kam and Lui, 2015). Additionally, Hoxb5 may regulate expression of key genes active in NCC development, notably *Foxd3* (Kam et al., 2014a) and *Phox2b* (Kam and Lui, 2015). The orthologous gene in zebrafish, *hoxb5b*, which is the primary ortholog in teleost fishes (Jarinova et al., 2008), was detected in differentiating NCC lineages at both 48 and 68 h post fertilization (hpf) (Howard et al., 2021), suggesting it may also play a role during zebrafish NCC development. While characterization of zebrafish *hoxb5b* mRNA expression *in situ* has been pervasively characterized in several early embryonic contexts, such as the mesoderm and limb buds (Kudoh et al., 2001; Jarinova et al., 2008; Waxman et al., 2008; Hortopan and Baraban, 2011; van der Velden et al., 2012), the functional role of *hoxb5b* with respect to NCC development had not yet been examined.

Here, we postulated that *hoxb5b* functions as a potential driver of vagal NCC development. We provide evidence that overexpression of *hoxb5b* is sufficient to grossly expand NCC populations throughout the zebrafish embryo, in addition to ectopic expansion of vagal domains marked by *foxd3* and *phox2bb*. The functional window of Hoxb5b activity was also restricted to a narrow developmental span, early during embryogenesis, rather than during NCC differentiation stages. The early expansion of NCC, however, did not lead to corresponding pan increases in NCC-derived tissues. Rather, elevated Hoxb5b activity expanded enteric neural progenitor cell pools along the gut, yet suppressed their subsequent expansion as they differentiated into enteric neurons, leading to overall fewer neurons along the gut. These data cumulatively support a model in which *hoxb5b* is a potent regulator of NCC expansion and cell number in zebrafish.

RESULTS

hoxb5b is Expressed in Post-Otic Vagal NCCs During Zebrafish Development

We examined *hoxb5b* expression in zebrafish embryos (Figure 1A) using whole mount *in situ* hybridization (ISH). At 32 hpf, *hoxb5b* was expressed bilaterally immediately posterior to the otic vesicle (post-otic), along

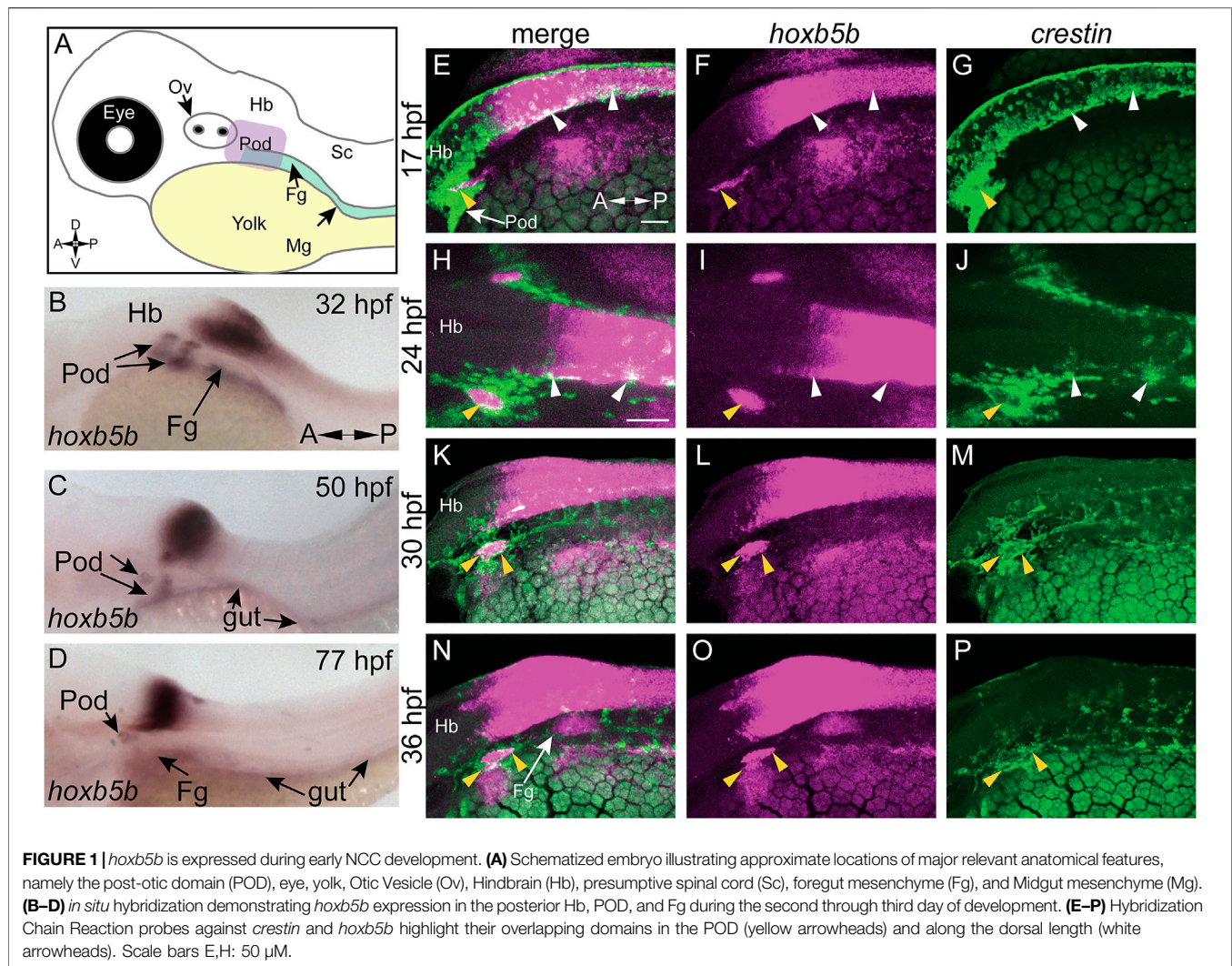
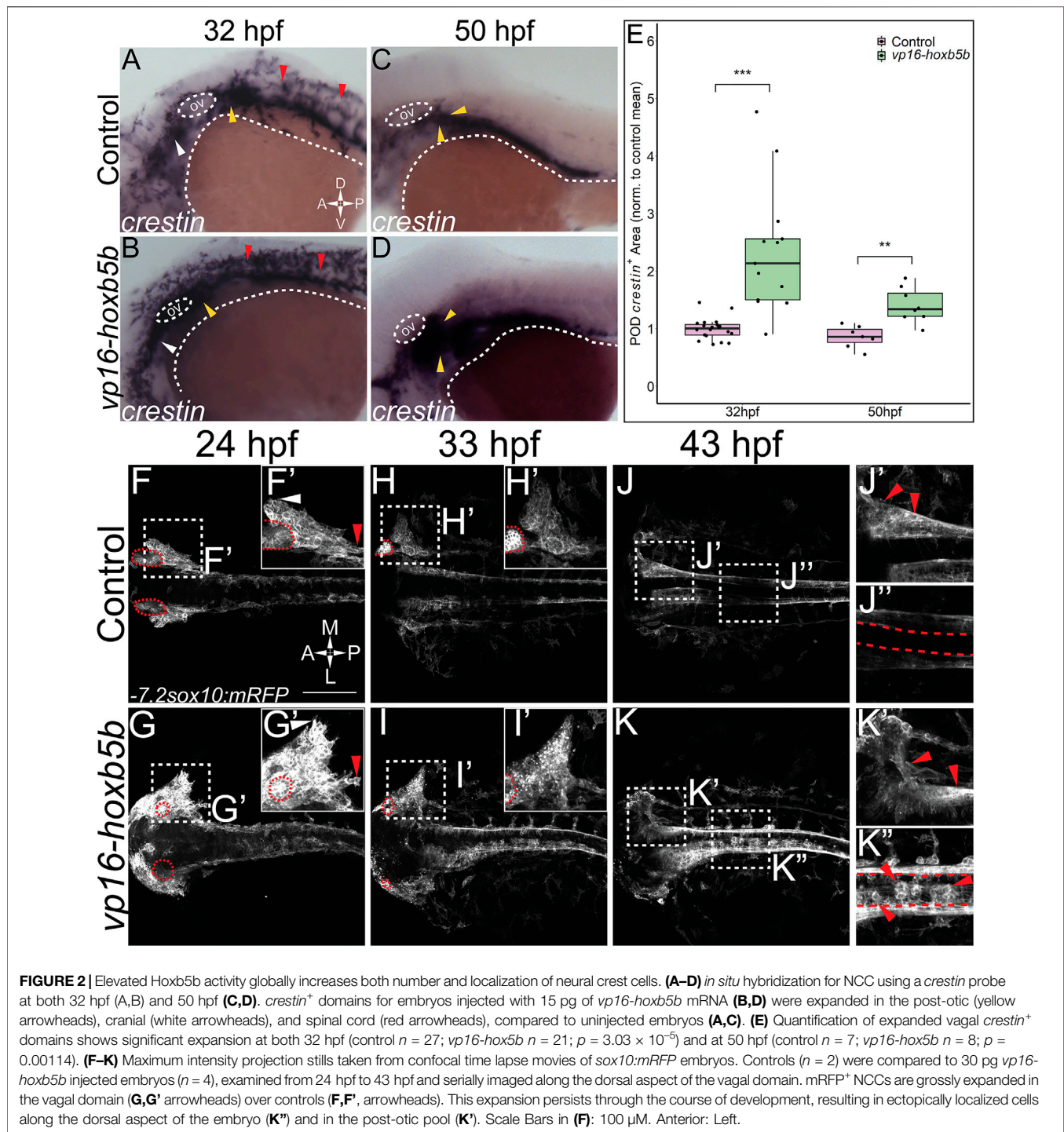


FIGURE 1 | *hoxb5b* is expressed during early NCC development. **(A)** Schematized embryo illustrating approximate locations of major relevant anatomical features, namely the post-otic domain (POD), eye, yolk, Otic Vesicle (Ov), Hindbrain (Hb), presumptive spinal cord (Sc), foregut mesenchyme (Fg), and Midgut mesenchyme (Mg). **(B–D)** *in situ* hybridization demonstrating *hoxb5b* expression in the posterior Hb, POD, and Fg during the second through third day of development. **(E–P)** Hybridization Chain Reaction probes against *crestin* and *hoxb5b* highlight their overlapping domains in the POD (yellow arrowheads) and along the dorsal length (white arrowheads). Scale bars E,H: 50 μ m.

the foregut, in the hindbrain, and anterior spinal cord (**Figure 1B**), as previously described (Jarínova et al., 2008). *hoxb5b* persisted in all three domains at 50 hpf (**Figure 1C**), though the post-otic domains (POD) were slightly restricted and the hindbrain/spinal cord expression gained a more defined posterior boundary. By 77 hpf, *hoxb5b* expression remained largely in the hindbrain and foregut, with diminished yet persistent expression in the POD (**Figure 1D**). Together, these ISH data reveal changing post-otic spatiotemporal expression patterns of *hoxb5b* during the first 4 days of development.

We next examined the relationship of *hoxb5b* expression to the vagal NCC population during NCC specification and migration phases. NCCs were assayed by using the zebrafish pan-NCC marker *crestin* (Luo et al., 2001), in combination with *hoxb5b*, via hybridization chain reaction (HCR) (Choi et al., 2010, 2016, 2018). At 17 hpf, *crestin*⁺/*hoxb5b*⁺ domains were present dorsally (**Figures 1E–G**, white arrowheads), as well as ventral-laterally, along a post-otic stripe (**Figures 1E–G**, yellow arrowhead), revealing that *hoxb5b* is

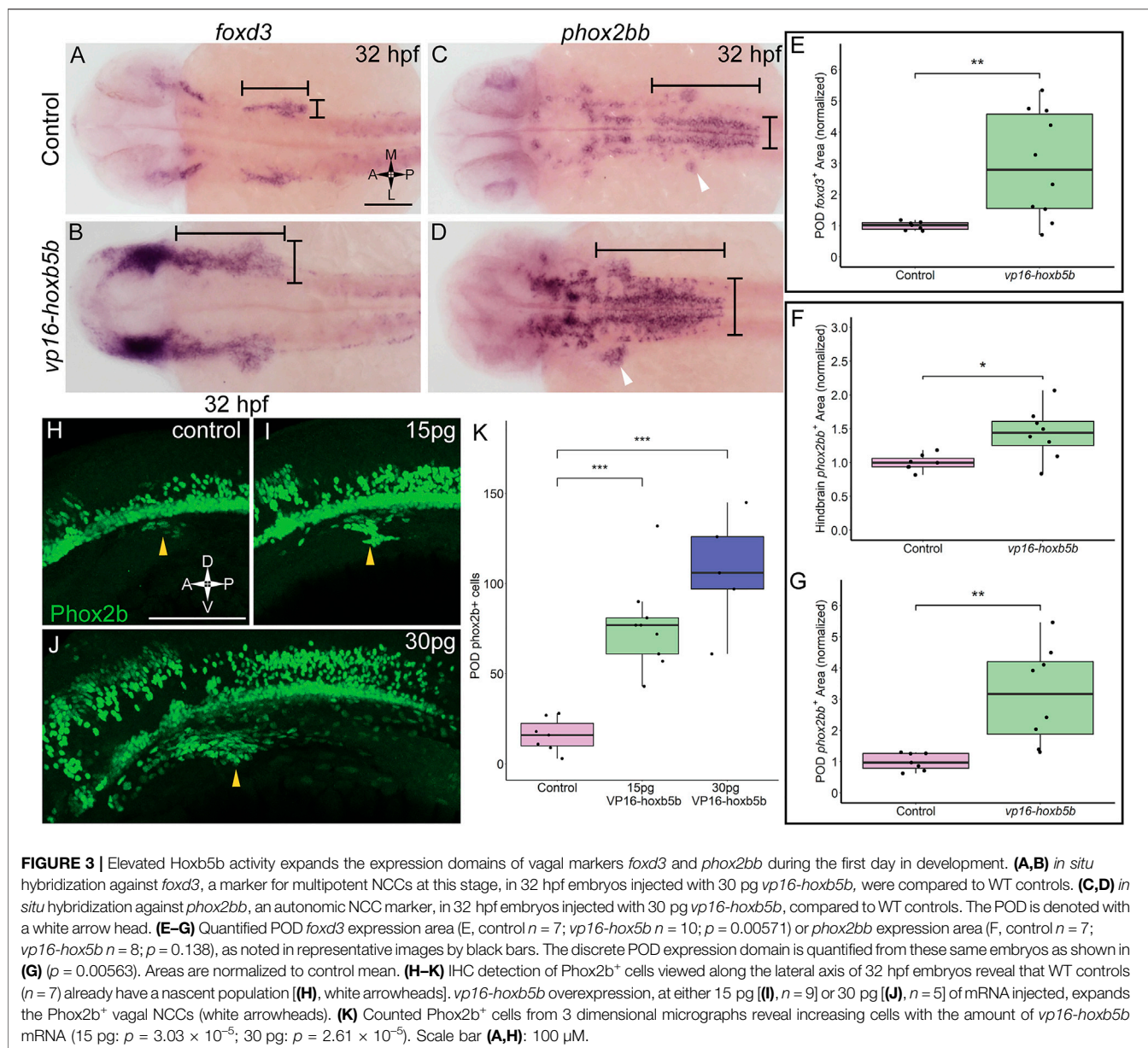
expressed within the POD vagal NCC population. *crestin*⁺/*hoxb5b*⁺ regions persisted by 24 hpf dorsally, in posterior hindbrain/anterior spinal cord axial levels (**Figures 1H–J**, white arrowheads). Concurrently at this stage, *hoxb5b* expression within the stripe became internalized within the POD vagal NCC population, marking the central area of this region, and highlighting several adjacent *crestin*⁺/*hoxb5b*⁺ domains (**Figures 1H–J**, yellow arrowhead). Between 30–36 hpf, the co-positive *hoxb5b*⁺/*crestin*⁺ stripe of POD vagal NCC persisted (**Figures 1K–P**, yellow arrowheads), and *crestin*⁺/*hoxb5b*⁺ regions were still observed along the dorsal neural tube. These data are consistent with our prior findings in which *hoxb5b* mRNA was present in posterior NCC at 48–50 hpf and 68–70 hpf (Howard et al., 2021). Collectively, the ISH and HCR data indicate that *hoxb5b* mRNA expression is coincident within the vagal NCCs area, persisting throughout the developmental window spanning NCC specification and well into their migration phase, highlighting *hoxb5b*'s potential role as a driver of vagal NCC development.



Elevated Hoxb5b Activity Globally Promotes Expanded Localization and Increased Number of NCC *in vivo*

While other work has focused exclusively on the loss of function of Hoxb5 related genes (Lui et al., 2008; Dalgin and Prince, 2021), we have sought to understand the gain of function role of *hoxb5b* in the context of NCC development.

To examine the possible role of *hoxb5b* in NCC, we employed a hyperactive *vp16-hoxb5b* fusion construct (Waxman et al., 2008; Waxman and Yelon, 2009). Injection of *vp16-hoxb5b* mRNA resulted in expansion of NCC, when compared to control embryos at 32 hpf, as assayed with an ISH probe against *crestin* (Figures 2A,B). The expansion in NCC territory was prominent in the pre-otic region (Figure 2B; white arrowheads), the POD (Figure 2B; yellow arrowheads)



and along the spinal cord-level of the trunk (**Figure 2B**; red arrowheads). Strikingly, post-otic expansion persisted along the dorsal-ventral and anterior-posterior axes well through NCC migration phases at 50 hpf (**Figures 2C,D**; arrowheads). Furthermore, quantification of the area occupied by POD NCCs corroborated the observed expansion of NCC localization (**Figure 2E**).

To better understand the spatiotemporal distribution of the increased NCC following *vp16-hoxb5b* expression, we utilized confocal microscopy to image *-7.2sox10:mRFP* transgenic embryos (referred to here as *sox10:mRFP*) (Kucenas et al., 2008), where NCC are labeled using a membrane bound RFP. Congruent with our prior findings (**Figures 2A,B**), at 24 and 33 hpf, confocal projections revealed *vp16-hoxb5b* expressing embryos exhibited broadened POD vagal NCC domains along

the anterior-posterior and medio-lateral axes (**Figures 2G,G',I,I'**; arrowheads), when compared to control embryos (**Figures 2F,F',H,H'**; arrowheads). This expansion was coupled with an increase in the number of POD NCC. By 43 hpf, *vp16-hoxb5b* expressing embryos displayed a striking expansion of the POD NCC, as well as a disruption of the overall architecture of the domain, which extended further laterally from the dorsal midline (**Figure 2K'**), than in control (**Figure 2J'**). Moreover, *vp16-hoxb5b* promoted ectopic accumulation of cells along the dorsal midline of the spinal cord (**Figure 2K'**), which were not observed in control embryos (**Figure 2J'**). Considered together, these data (**Figure 2**) indicate that elevated Hoxb5b activity alters NCC localization along the embryo as well as expanding their cell number.

Elevated Hoxb5b Activity is Sufficient to Expand Vagal NCC Marker Expression

That *vp16-hoxb5b* expressing embryos contained an overabundance of NCC, and that the overproduced NCC were prominently enriched in the vagal axial levels suggests that excess Hoxb5b activity influences vagal NCC development in zebrafish. To examine if vagal NCC specification was altered following excess Hoxb5b activity, we assayed the expression of canonical marker genes of the vagal NCC, *foxd3* (Lister et al., 2006) and *phox2bb* (Elworthy et al., 2005). At 32 hpf, *foxd3* expression serves as an indicator of multipotent NCC while *phox2bb* indicates NCCs which are now specified to an autonomic neural lineage, particularly the ENS (Pattyn et al., 1999; Uribe and Bronner, 2015). *vp16-hoxb5b* expression was sufficient to widen *foxd3* expression domains at 32 hpf, principally along the anterior-posterior and mediolateral directions in the vagal region, when compared to control expression patterns (Figures 3A,B; black bars). We found that *vp16-hoxb5b* expression expanded the POD *foxd3*⁺ area, leading to a 1.95 fold increase in the mean domain size compared to controls (Figure 3E). Additionally, *phox2bb* was also greatly expanded in response to increased Hoxb5b activity along the hindbrain (Figures 3C,D; black bars), with expansion uniformly in both the anterior-posterior and mediolateral axis, similar to the expansion of the *foxd3*. Measuring the hindbrain *phox2bb*⁺ domain, we observed a 43% increase in the *phox2bb* expressed area throughout the hindbrain following elevated Hoxb5b (Figure 3F). Lastly, POD *phox2bb* expression was dramatically altered by elevated Hoxb5b (Figures 3C,D; white arrow heads), with a 2.14 times mean increase in domain size compared to wild-type controls (Figure 3G). In all, these data indicate that elevated Hoxb5b activity drastically expands vagal NCC marker expression along the embryo.

In support of the specific expansion of POD localized *phox2bb* expression, we also observed a corresponding increase in the number of Phox2b⁺ cells, *via* whole mount fluorescent Immunohistochemistry (IHC), using an antibody against Phox2b (Supplementary Figures S1A–C; Figure 3). At 32 hpf, Phox2b⁺ cells were observed in the POD, with 16 cells on average (Figure 3L; arrowhead, Figure 3K). Overexpression of Hoxb5b stimulated a dramatic expansion of POD Phox2b⁺ cells (Figures 3I,J; arrowheads). The increase in POD Phox2b⁺ cells was also concordant with an increase in *vp16-hoxb5b* dosage, with 77 and 107 mean POD Phox2b⁺ cells per animal detected following injection with either 15 pg or 30 pg of mRNA, respectively (Figure 3K). The quantifiable increase in POD Phox2b⁺ cells is confirmatory of our prior qualitative observations regarding increased cell number (Figure 2) and positions Hoxb5b as a potent driver of NCC number and localization.

Hoxb5b Overexpression Increases NCC Production During Early NCC Development

While we observed supernumerary NCCs ectopically localized, and expanded expression of vagal NCC specification factors following global expression of *vp16-hoxb5b* mRNA, exactly when during NCC development Hoxb5b may exert its

influence was still unclear. To investigate the potential temporal role(s) of Hoxb5b during NCC development, we created and utilized a novel transgenic line, Tg (*hsp70l:EGFP-hoxb5b;cryaa:dsRed*)^{ci1014} (hereafter referred to as *hsp70l:GFP-hoxb5b*), which enables pan ectopic expression of a GFP-Hoxb5b protein fusion under the thermally inducible *hsp70l* promoter (Kwan et al., 2007) (Figure 4A). The transgene can then be activated by rapidly transferring embryos to warm 37°C culture conditions, which drives strong global expression of the EGFP-Hoxb5b fusion protein throughout the embryonic tissues (Supplementary Figure S2A). EGFP-Hoxb5b demonstrated robust and distinctive nuclear localization, which was still detectable over 24 h after embryos were returned to 28°C (Supplementary Figures S2B,C).

Two early phases in NCC development were tested, with heat shocks conducted starting either at 14 hpf, during NCC specification, or 22 hpf, early during the migratory span of posterior NCCs (Figure 4B). After heat shock at 14 hpf, whole mount ISH at 24 hpf showed enlargement of *crestin*⁺ NCC domains in GFP-Hoxb5b⁺ embryos, over the GFP-Hoxb5b⁻ sibling controls (Figures 4C,D), particularly prevalent in the POD NCC (Figure 4D; yellow arrowheads). This increase in area was also accompanied by a qualitative increase in the number of *crestin*⁺ cells along the posterior dorsal length of the embryo, similar to the phenotype observed in the previous Hoxb5b mRNA overexpression assays (Figures 2A–E). Quantified area of *crestin*⁺ PODs confirmed the expansion of vagal NCCs (Figure 4I). Additionally, subtle expansion of cranial NCCs (Figures 4C,D, white arrowheads) and pre-otic NCCs (Figures 4C,D, red arrowheads) was also observed, though far less striking than that of the vagal population at this stage. These data indicate that NCC localization during early specification phase of NCC development is receptive to Hoxb5b activity.

GFP-Hoxb5b induction at 22 hpf also increased *crestin* staining by 26–28 hpf throughout the POD (Figures 4E–H, yellow arrowheads), which was especially prominent in the NCCs most proximal to the otic vesicles (Figures 4G,H, red arrowheads). As in the heat shock at 14 hpf, increased NCC localization was also observed in GFP-Hoxb5b⁺ embryos across the cranial NCC populations (Figures 4E–H; white arrowheads). This induction of GFP-Hoxb5b also significantly expanded measurable vagal NCC area (Figure 4J), with a 26% mean increase in area compared to GFP⁻ siblings. The expansion in area coupled with the increase in *crestin* staining replicates the results obtained via the microinjection assays presented in Figure 2, albeit more subtly, as well as indicates that 14–22 hpf is a critical period during which Hoxb5b is sufficient to alter NCC localization in the developing vertebrate body.

Increased Hoxb5b Alters Specific Vagal NCC-Derived Tissues

Due to the multipotent nature of NCC, it is possible a wide diversity of tissues can be affected by even a small perturbation in NCC development. Because we observed an overproduction of NCC following increases in Hoxb5b activity, we wondered if

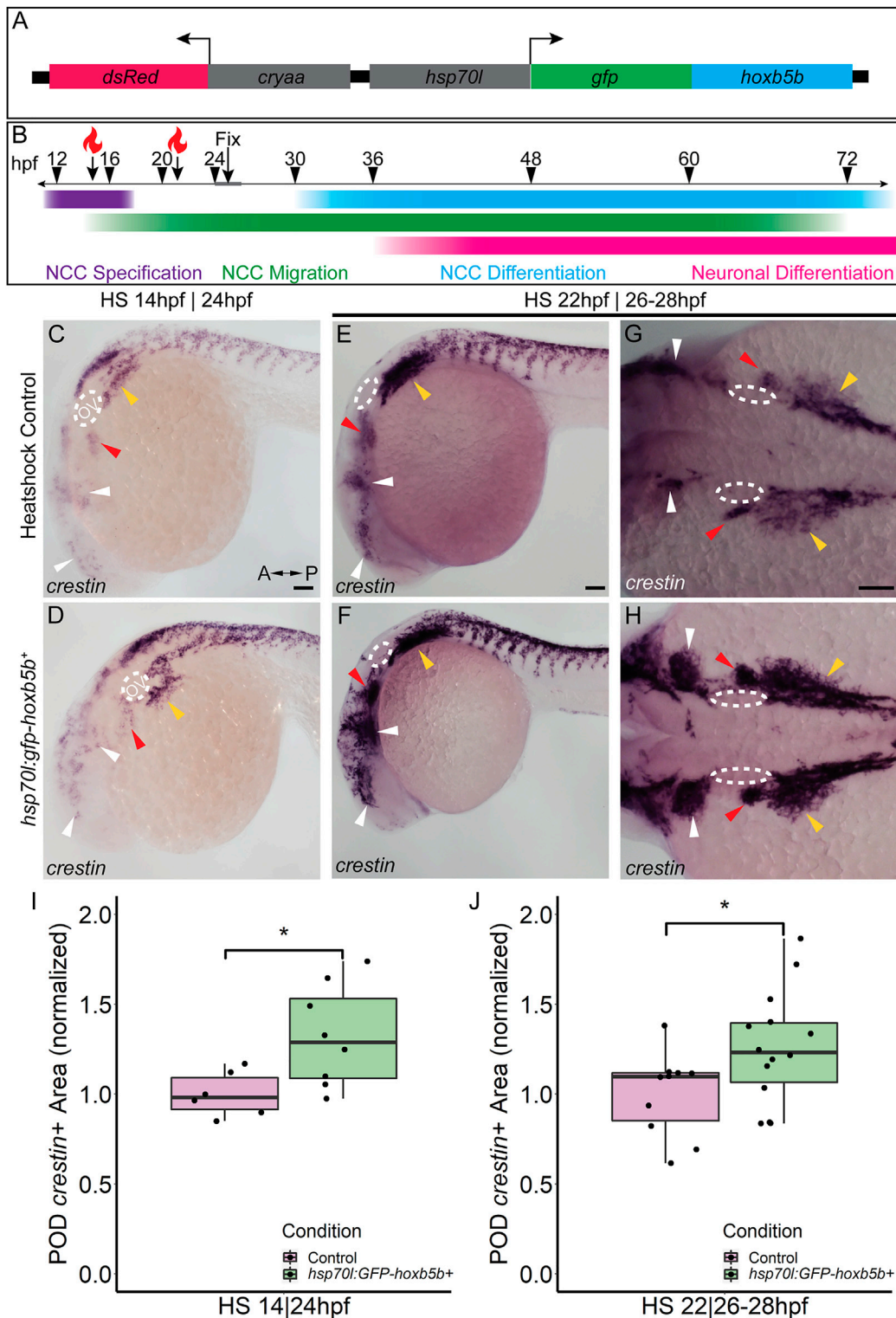


FIGURE 4 | Temporally controlled overexpression of Hoxb5b during the first day in development is sufficient to expand the neural crest pool. **(A)** Schematized model of the *hsp70l:gfp-hoxb5b;cryaa:dsRed* genetic construct. **(B)** Illustration depicting specific periods of heat shock for embryo groups relative to classical hallmarks of zebrafish NCC development. **(C,D)** *in situ* hybridization using a probe for *crestin* in *hsp70l:GFP-hoxb5b*⁺ embryos heat shocked at 14 hpf and fixed at 24 hpf, compared to GFP⁻ sibling controls treated in parallel. Dramatic expansion of the POD can be seen (yellow arrowheads) in the Hoxb5b overexpressing embryos, while more subtle expansion is noted in the cranial NCC (white arrowheads) and pre-otic crest (red arrowheads). **(E-H)** Similar to **(C,D)** *in situ* hybridization with a *crestin* (Continued)

FIGURE 4 | probe in *hsp70l:gfp-hoxb5b* and GFP- sibling controls heat shocked at 22 hpf and fixed at 26–28 hpf, examining both *crestin*⁺ domains both laterally (**E,F**) and dorsally (**G,H**). (**I,J**) Graphs depicting areas occupied by *crestin* staining in both GFP- control and Hoxb5b overexpressing embryos. Hoxb5b overexpression at 14 hpf was sufficient to expand NCC localization and qualitatively NCC number (**I**), control $n = 6$; *hsp70l:GFP-hoxb5b*⁺ $n = 8$; $p = 0.0234$. A later heat shock at 22 hpf—fixation at 26–28 hpf, also expanded vagal NCC localization (**J**), control $n = 10$; *hsp70l:GFP-hoxb5b*⁺ $n = 14$; $p = 0.0398$, and increased *crestin* staining, indicative of an increase in NCC number. Scale bars (**C,E,G**): 100 μ M

downstream NCC derivatives were also affected. Therefore, we first investigated the effect of *vp16-hoxb5b* expression on vagal and trunk NCC-derived cell types; including, pigment cells (melanophores and iridophores) and neuronal derivatives. Embryos expressing *vp16-hoxb5b* were able to produce pigment cells without appreciable differences (Supplementary Figures S4A–D). Both dorsal root ganglia (DRG) and Superior Cervical Ganglion (SCG) are derived from the vagal/trunk NCC pool (Durbec et al., 1996). Neurons comprising the DRG and SCG were largely normal following *vp16-hoxb5b* injection (Supplementary Figures S4E–H).

We next assayed the NCC-derived cell population along the gut length (Figure 5A), enteric neural progenitors, which typically migrate to the midgut level by 2 dpf and will have colonized the hindgut by 3 dpf, giving rise to neurons of the enteric nervous system (Elworthy et al., 2005; Ganz, 2018). We found that by 50 hpf, Phox2b⁺ enteric neural progenitors significantly increased after *vp16-hoxb5b* expression (Figures 5C,D), compared to the controls (Figure 5B). Counting Phox2b⁺ cells in the POD and along the gut tract (Figures 5B–D; white dashes), revealed the number of cells trended with increasing amount of *vp16-hoxb5b* mRNA injected (Figure 5E), consistent with the phenotype at 32 hpf (Figures 3H–J). The supernumerary enteric neural progenitors were observed together with their accumulation along the foregut (Figures 5B–D; yellow arrowheads) and in the POD (Figure 5F), though an increase in the number of cells was also observed at the end of the enteric migration chain along the midgut (Supplementary Figure S4I; Figures 5C,D; white arrowheads). The increase in cells was uniform across the gut tract, with no change in the fraction of Phox2b⁺ cells found in the POD or gut mesenchyme after Hoxb5b perturbation (Supplementary Figure S4J). These findings indicate that elevated Hoxb5b elicits a global increase in enteric neural progenitor number through the first 2 days of development.

To determine if the supernumerary enteric cells were capable of differentiating into neurons later in development, we utilized *-8.3phox2bb:kaede* transgenic embryos which label enteric progenitors during their early neuronal differentiation (Harrison et al., 2014). Surprisingly, despite the increase in enteric progenitors at 50 hpf, enteric neurons by the 3 dpf were dramatically decreased in *vp16-hoxb5b* expressing embryos compared to controls. Kaede⁺ cells successfully colonized the gut length by 3 dpf in control embryos (Figure 5G; white arrowhead), many cells of which (42%) also co-expressed the pan neuronal marker Elavl3/4 (Figures 5G,K,L), signaling the onset of neuron differentiation. In contrast, *vp16-hoxb5b* expressing embryos at both doses displayed a drastic loss of Kaede⁺ and Elavl3/4⁺ enteric cells (Figures 5J,K), with the remaining Kaede⁺ cells failing to localize

past the level of the midgut (Figures 5H,I; white arrowheads). The fraction of Elavl3/4⁺/Kaede⁺ cells in both *vp16-hoxb5b* expressing conditions were reduced, at 0.31 and 0.28 respectively, when compared to control at 0.42 (Figure 5L). While not reaching significance, when these data are taken together with the significant reduction in total enteric cell numbers along the gut (Figures 5J,K), they likely indicate that general enteric progenitor pool depletion along the gut affects subsequent proper numbers of enteric neurons, following elevated Hoxb5b expression. Overall, these results suggest that while supernumerary enteric neural progenitors are present at and before 2 dpf after elevated Hoxb5b, they largely depleted by the 3 dpf.

Hoxb5b influences Enteric Colonization During Early Developmental Stages

In order to ascertain the timing during which excess Hoxb5b activity affects enteric nervous system development, we again leveraged the *hsp70l:GFP-hoxb5b* fish line. Embryos were heat shocked during NCC specification (14 hpf), migration (21 hpf), or differentiation (48 hpf), and all were fixed at 3 dpf, as schematized in Figure 6A. Embryos were assessed for enteric neuron abundance and localization via wholemount IHC, where Elavl3/4⁺ cells were counted along the gut tract (same region as in Figure 5A, box). When heat shocked at 14 or 21 hpf, GFP-Hoxb5b⁺ embryos formed significantly fewer Elavl3/4⁺ cells, when compared to their GFP-Hoxb5b⁻ sibling heat shock controls (Figures 6B–E,H). After heat shock at 48 hpf, GFP-Hoxb5b⁺ embryos did not significantly vary in number of Elavl3/4⁺ cells (Figures 6F–H). The distribution of Elavl3/4⁺ cells was weighted more heavily toward the midgut, though cells could be detected along the entire length of the gut in GFP-Hoxb5b⁺ embryos. This genetically encoded elevation of Hoxb5b activity during early NCC developmental phases corroborated the abrogation in Elavl3/4⁺ cells resulting from *vp16-hoxb5b* mRNA injection. Overall, these data indicate that the ability of GFP-Hoxb5b to affect enteric neuron number is limited to early stages of NCC development, but not thereafter.

Excess Hoxb5b Leads to Stalled Enteric Nervous System Development

We had thus far discovered that Hoxb5b was sufficient to strongly increase NCCs at 30 and 50 hpf, but suppressed the number of enteric neural progenitor cells by 3 dpf. The loss in cells could easily be explained by an acute wave of cell death during enteric neural progenitor migration. We tested this hypothesis with whole mount IHC probing for activated Caspase-3, a marker for apoptotic cells (Sorrells et al., 2013), as well as Phox2b to label

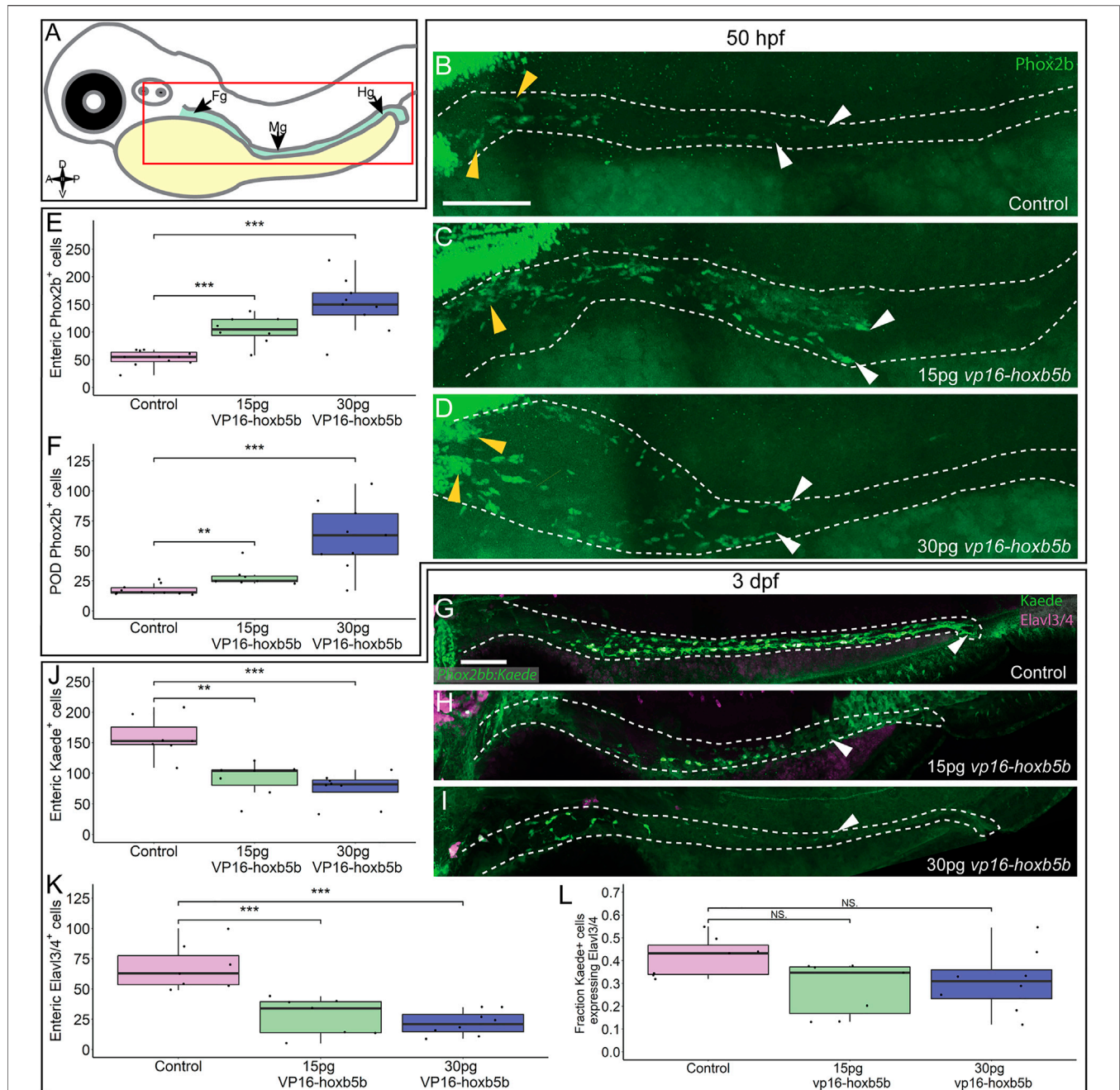
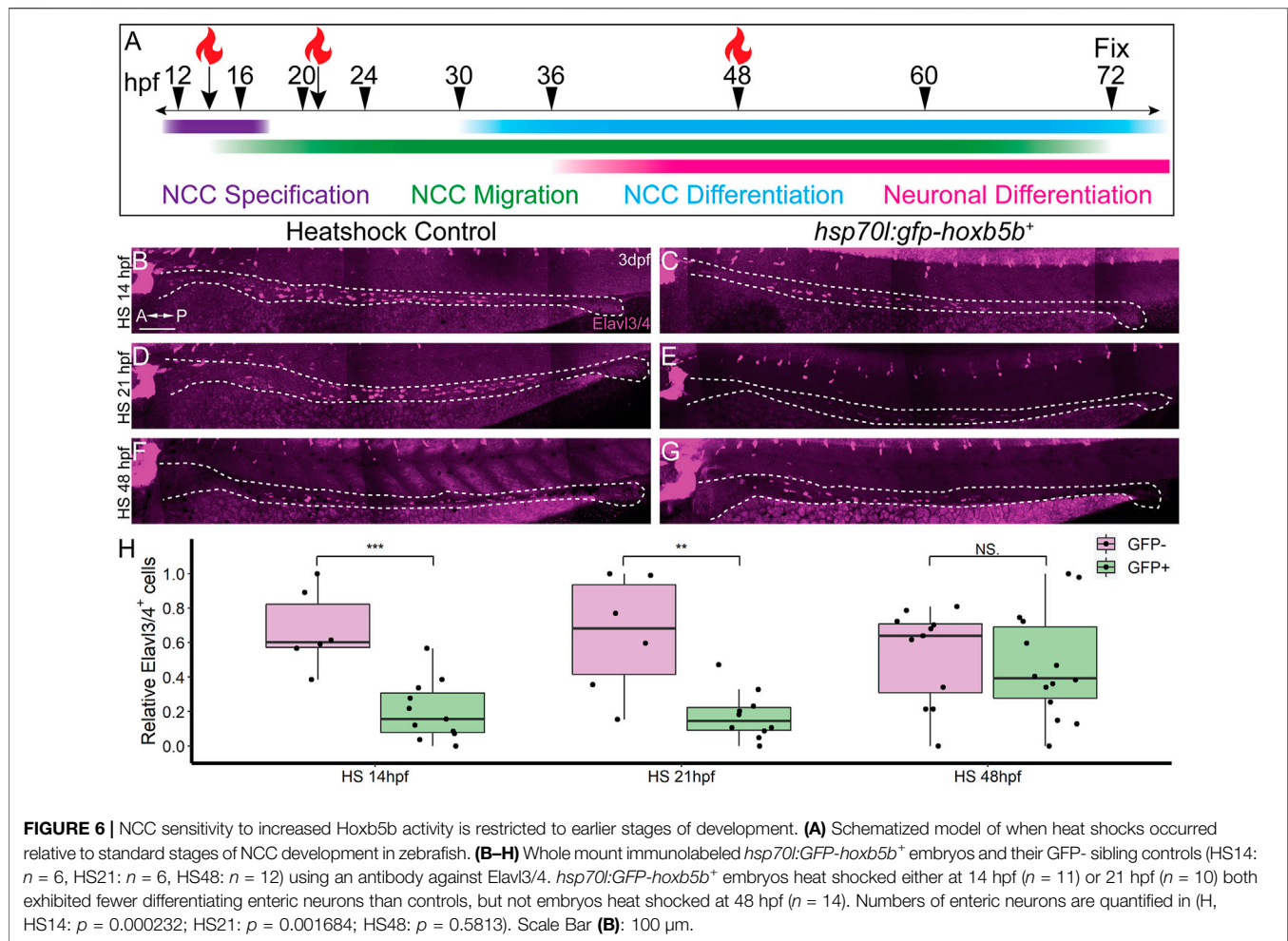


FIGURE 5 | Hoxb5b is sufficient to expand early enteric neural progenitors. **(A)** Schematized model of a zebrafish embryo highlighting the region of the gut tube, which is imaged in the following panels. **(B–D)** Whole mount IHC for Phox2b in 50 hpf control embryos **(B)**, $n = 10$] compared to embryos injected either with 15 pg **(C)**, $n = 7$] or 30 pg **(D)**, $n = 9$] of *vp16-hoxb5b* mRNA. Yellow arrow heads indicated POD localized Phox2b⁺ cells, white arrows designate terminal end of enteric NCC chain, which falls within the gut tract outlined with white dashes. **(E,F)** Quantified cell numbers from the same animals reveal a coordinate increase in Phox2b⁺ along the gut axis at 50 hpf trending with increasing *vp16-hoxb5b* mRNA amounts **(E)**, 15 pg: $p = 2.834 \times 10^{-5}$; 30 pg: $p = 0.00318$]. Additionally, the number of Phox2b⁺ cells restricted to the POD also increased in response to elevated Hoxb5b activity **(F)**, 15 pg: $p = 0.00328$; 30 pg: $p = 0.00068$]. **(G–I)** Whole mount IHC on 3 dpf *-8.3phox2bb:kaede* embryos with antibodies against Elavl3/4 and Kaede, marking the enteric NCC lineage cells in *vp16-hoxb5b* overexpressing animals (15 pg $n = 8$; 30 pg $n = 7$) compared to uninjected sibling controls ($n = 7$). **(J–L)** Quantification of the number of enteric neural progenitors **(J)**, 15 pg: $p = 0.00011$; 30 pg: $p = 4.09 \times 10^{-5}$) and differentiating enteric neurons **(K)**, 15 pg: $p = 0.001352$; 30 pg: $p = 0.0001042$) at 3 dpf show decreasing numbers of both cell populations. However, the total fraction of differentiating (Hu⁺) NCC-derived Kaede⁺ cells unchanged following elevated Hoxb5b activity **(L)**, 15 pg: $p = 0.01282$; 30 pg: $p = 0.102$]. Scale Bar **(B,G)**: 100 μ M.

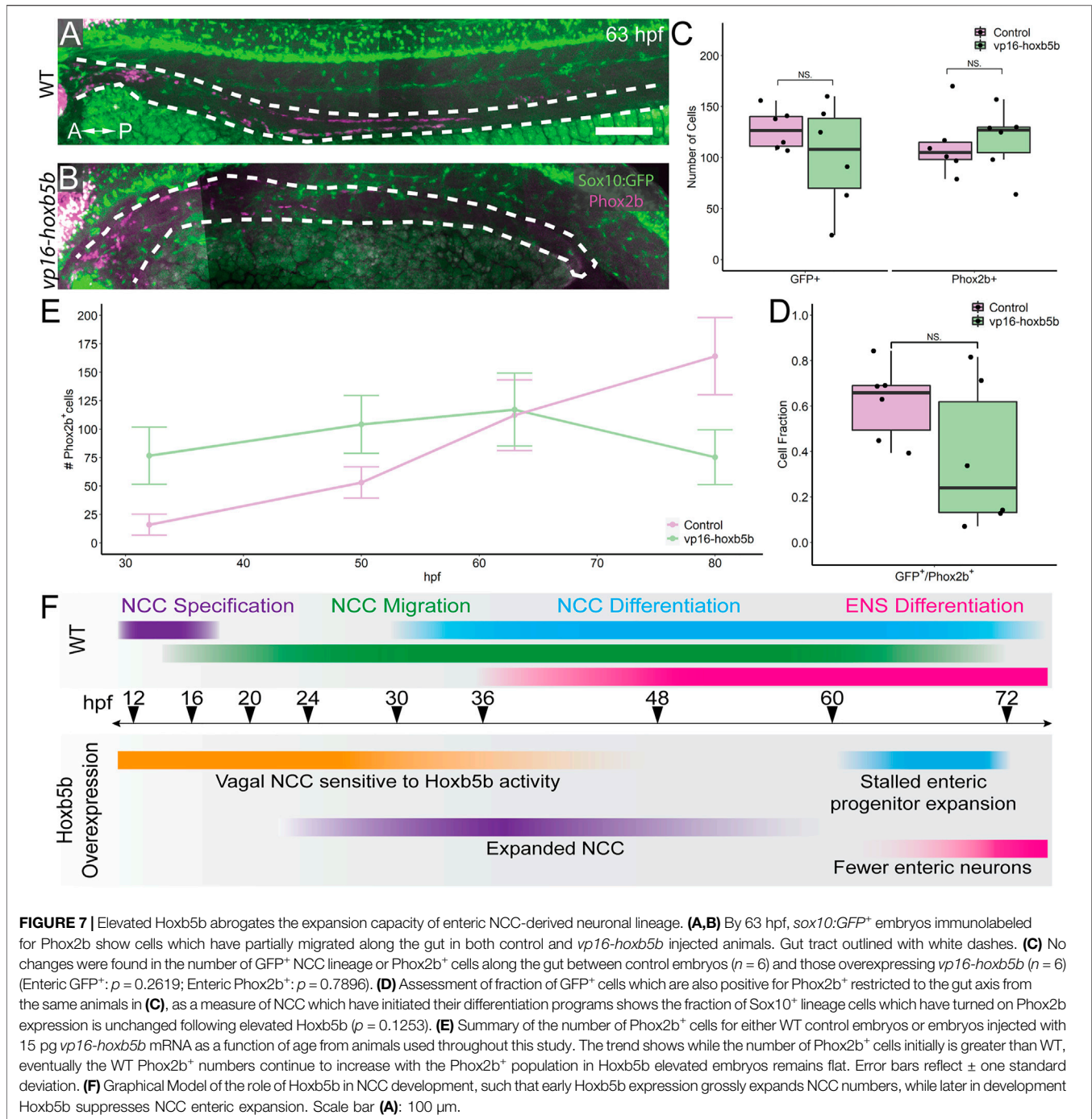


enteric neural progenitors. In addition, we also conducted these experiments in the Tg (*-4.9sox10:eGFP*) embryos (hereafter referred to as *sox10:GFP*) (Carney et al., 2006), which marks migratory NCCs with cytoplasmic GFP, and relying on residual GFP signal post fixation to label the recently *sox10*⁺ enteric neural progenitor cells, as we have previously (Howard et al., 2021). Notably, Caspase-3⁺ cells were rare in all control tissues examined from 33 to 66 hpf (**Supplementary Figures S3A,C,E,G**). While small patches of apoptotic cells can be found proximal to the POD at 33 hpf and 55 hpf (**Supplementary Figures S3B,D**), there was not a detectable onset of cell death between 55 and 66 hpf along the entire vagal and gut region (**Supplementary Figures S3F,H**) to support the loss of enteric neural progenitors through apoptosis following Hoxb5b overexpression.

We next examined the progenitor state of enteric cells at 63 hpf, a window of development prior to the 3 dpf cut off, but after the 50 hpf NCC expansion noted previously. To this end, we asked if *sox10:GFP*⁺ and/or Phox2b⁺ cell numbers were reduced along the gut at 63 hpf. Intriguingly, *vp16-hoxb5b* did not lead to a significant change in the total number of GFP⁺ cells along the gut tube at 63 hpf (**Figures 7A–C**). Similarly, there was no change in the number of Phox2b⁺ cells, compared with control embryos (**Figure 7C**). This

was in contrast to our earlier observation that enteric Phox2b⁺ cells were increased at 50 hpf (**Figure 5**). Furthermore, the fraction of *sox10:GFP*⁺ cells expressing Phox2b was unchanged (**Figure 7D**). Therefore, we found that by 63 hpf the enteric progenitors exhibited enteric differentiation capacity, despite their decreased abundance in the presence of excess Hoxb5b.

That we observed increased Phox2b⁺ cells at 32 and 50 hpf, yet saw a dampening of their numbers by 63 hpf, this suggested that the kinetics of enteric progenitor expansion may have been adversely affected following elevated Hoxb5b. Plotting the total number of Phox2b⁺ cells counted from each developmental stage assayed throughout this study (**Figure 7E**) revealed a steady increase in control Phox2b⁺ cells with developmental age, whereas Hoxb5b overexpressing animals presented a stalled curve at 63 hpf. As we previously have shown that the enteric cells are not cleared by apoptosis during the 63–80 hpf transition, these results indicated that Hoxb5b activity modulates enterically-fated NCC capacity to expand as a population along the gut. The Hoxb5b-dependent precocious expansion of NCC leads to a fixed number of available progenitors which are then unable to expand in sufficient numbers to lead to proper ENS formation. These findings position Hoxb5b as a fine-scale regulator of enteric NCC number.



DISCUSSION

We discovered that throughout the course of NCC specification and migratory phases, *hoxb5b* is expressed within the vagal NCC domain along the post-otic/posterior zebrafish embryo. Enhancement of Hoxb5b activity was sufficient to dramatically expand NCC localization patterns, as well as their number, along the embryo. The expansion of NCCs was also accompanied by domain expansions in vagal NCC marker genes *phox2bb* and *foxd3*. Temporally-restricted pulses of ectopic Hoxb5b during

early vagal NCC developmental phases was sufficient to swiftly expand vagal NCC populations, which also persisted well into the second day in development. While many vagal NCC derivatives were unaltered by 3 dpf, NCC derivatives along the enteric neural trajectory were dramatically impacted. While we observed an increase in enteric neural progenitors along the developing gut tube at 50 hpf, they failed to expand and colonize the gut efficiently, resulting in a marked decrease in the number of enteric neurons. The decrease in enteric neural progenitors following Hoxb5b induction appears to be due to a Hoxb5b-

dependent modulation of the colonization capacity of enteric neural progenitors. Cumulatively these data position Hoxb5b as a potent regulator of NCC patterning and number during early embryonic development (**Figure 7F**).

The potential involvement of Hoxb5b in zebrafish NCC development has been suggested by previous expression analyses, with discrete expression along the dorsolateral neural tube and in the post-otic domain, posterior to rhombomere 8 (Kudoh et al., 2001; Jarinova et al., 2008; Waxman et al., 2008; Barsh et al., 2017). Additional expression domains are found within the lateral plate mesoderm and foregut by 24 hpf (Dalgin and Prince, 2021). As identified in a single cell atlas of posterior zebrafish NCC lineages at 48–50 and 68–70 hpf, *hoxb5b* was among the most pervasively expressed transcripts encoding for a Hox transcription factor in both the NCC and in neural fated lineages (Howard et al., 2021). Extending this prior work, our HCRs show for the first time at high resolution the persistent expression of *hoxb5b* in zebrafish posterior (post-otic) NCC through the early course of their development.

In our zebrafish model, despite the regional potential exhibited by NCCs (Rocha et al., 2020), elevated Hoxb5b uniformly expanded cranial, vagal, and trunk NCC progenitors, though more robustly among the posterior NCC populations. Whether the Hoxb5b-dependent increase in NCCs is driven by increased NCC specification from the neural tube or through upregulation of NCC proliferation remains unresolved and was beyond the current scope of this study. Regardless of the underlying mechanism, these findings clearly indicate that Hoxb5b participates in NCC development from an early position in the NCC gene regulatory network (Simoes-Costa and Bronner, 2016; Martik and Bronner, 2017). Further, the rapid sensitivity of vagal NCC to temporally restricted pulses of elevated Hoxb5b suggests competency of these cells to abruptly respond to Hox activity early in their development. Indeed, early NCCs appear sensitive not only to Hox mediated activity but also the amount of Hoxb5b present. In our injection experiments, POD NCCs increased coordinately with amount of *vp16-hoxb5b* mRNA delivered. As such, the number of cells fated in select NCC lineages, such as the enteric NCCs, appear to be influenced not only by the activation of Hoxb5b-dependent activity, but also in part through the levels of Hoxb5b expression. From data derived across multiple animal models, Hoxb5b and its orthologues are known to be under control of several classical morphogenic signals, including WNTs (Lengerke et al., 2008), NOTCH (Hortopan and Baraban, 2011), and Retinoic Acid (Waxman et al., 2008), which enables fine spatiotemporal tuning of the levels of Hox expression. Summarily, our data thus illuminate a model in which Hoxb5b serves a potent regulator of posterior NCC identity and cell number, dependent on additional unspecified cofactors as well as its expression level.

Our findings regarding Hoxb5b in zebrafish NCC is complementary to and extends the developmental understanding of mammalian Hoxb5. For example, dominant negative suppression of Hoxb5 activity in NCC lineages led to a depletion of several NCC-derived cell populations including DRGs, pigment cells, as well as enteric neural progenitors (Lui

et al., 2008; Kam et al., 2014b). Complementing these prior loss of function studies, our gain of function data indicates that elevated Hoxb5b activity is sufficient to induce expansion of vagal NCC progenitors—that paradoxically also leads to severe ENS hypoganglionosis. While we did not observe corresponding changes in DRG and pigment populations in our experiments; early enteric progenitors were dramatically increased in response to Hoxb5b activity along the gut, prior to the onset of neurogenesis, yet failed to properly execute enteric neuronal differentiation. Somewhat counterintuitively, the increase in POD NCCs following increased Hoxb5b activity did not correspondingly manifest a pan increase in vagal-derived NCC lineages. While many vagal-derived lineages exhibited no discernable phenotypic change, we observed a dramatic decrease in the number of enteric neurons in animals with elevated Hoxb5b activity. The shift in abundance of enterically fated cells in embryos overexpressing Hoxb5b was not the result of NCC-specific apoptosis or abrogated differentiation potential. Indeed, there was no change in fractions of enteric NCCs which had initiated differentiation programs following elevated Hoxb5b. Rather this tissue specific cell decrease appears to be caused by a late-onset suppression of enteric neuroblasts expansion. Assays for apoptosis-mediated cell death revealed limited tissue death, which was not restricted to NCC populations. While we did not test cell loss by other modes of death, such as necrosis or pyroptosis, the numbers of enteric NCC-derived cells were more consistent with the arrest of cell division as opposed to changes in cell survival. The insufficiency of ectopic Hoxb5b to expand the DRG and pigment lineages suggests a separate regulatory mechanism for Hoxb5b gain of function activity in enteric NCC.

Several possible frameworks may explain the differential role of Hoxb5b to expand early NCCs but abrogate their later expansion in the ENS. First, the differential role may be correlated with the temporally dynamic expression of additional co-factors, such as other Hox or TALE-family transcription factors within the ENS lineage. TALE-family factors in particular, such as Meis3 (Uribe and Bronner, 2015), or other factors such as Pbx3 (Di Giacomo et al., 2006) are both expressed within the early enteric neural lineage and may cooperate with Hoxb5b to facilitate functional specificity. Additional reflection on the emerging numerous descriptions of combinatorial “Hox Codes” which define NCC identity (Parker et al., 2019; Soldatov et al., 2019; Howard et al., 2021), reported functional similarity in certain tissues (Jarinova et al., 2008), as well as complex regulatory relationship between various members of the Hox gene family (Zhu et al., 2017), the prospect of a shared sensitivity in enteric NCCs to Hoxb5b and other posterior Hox transcription factors is possible, though beyond the context of this study. Another alternative hypothesis to explain Hoxb5b’s differential role may be related to the precociousness of the expansion of neural crest itself. As more NCCs accumulate earlier in development, temporally restricted signals may be insufficiently timed to signal for NCCs to continue to expand in number. While the underlying mechanism remains to be fully elucidated, when the data are considered together with mammalian suppression of activity studies referenced above,

our gain of function results suggest that the vertebrate embryo is exquisitely sensitive to perturbations in Hoxb5 activity, where either elevations or reductions in Hoxb5 lead to severe ENS defects. Collectively, we have discovered evidence in support of a model in which Hoxb5b plays an important role in NCC development, demonstrating the capacity to both expand vagal NCC localization and numbers. While additional questions still remain, these findings greatly inform our understanding of the role of posterior Hox genes in NCC development.

MATERIALS AND METHODS

Zebrafish Husbandry and Transgenic Lines

Synchronously staged embryos for each experiment were collected via controlled breeding of adult zebrafish. After collection, embryos were maintained in standard E3 media at 28°C until 24 h post fertilization (hpf), then transferred to 0.003% 1-phenyl 2-thiourea (PTU)/E3 solution (Karlsson et al., 2001), with the exception of larvae used to assay pigmentation, which were cultured in E3 media only. Transgenic embryos for the Tg (-4.9*sox10:EGFP*)^{ba2Tg} (Carney et al., 2006) and Tg (-7.2*sox10:mRFP*)^{vu234} (Kucenas et al., 2008) were generally sorted between 17–28 hpf for fluorescence while Tg (*hsp70l:EGFP-hoxb5b;acry:dsRed*)^{ci1014} and Tg (-8.3*phox2bb:kaede*) (Harrison et al., 2014) embryos were sorted for transgenic expression between 60–78 hpf. Tissue was collected from embryos out of their chorions at the stage noted in each experiment as described in (Ibarra-García-Padilla et al., 2021). All work was performed under protocols approved by, and in accordance with, the Rice University Institutional Animal Care and Use Committee (IACUC).

Generation of the Tg (*hsp70l:EGFP-Hoxb5b*) Transgenic Line

To generate EGFP-Hoxb5b, *egfp* was fused to the 5'-end of zebrafish *hoxb5b* with PCR. A sequence encoding a 7 amino acid linker was incorporated and the *hoxb5b* ATG was deleted to prevent alternative transcriptional initiation of *hoxb5b* downstream. To generate the *hsp70l:EGFP-Hoxb5b* transgene, standard Gateway methods were used (Kwan et al., 2007). The transgene includes a *EGFP-Hoxb5b* middle-entry vector and the reported *p5E-hsp70l* 5'-Entry and *p3E-polyA* 3'-entry vectors (Kwan et al., 2007), which were incorporated into the *pDestTol2-acry:dsRed* vector (Mandal et al., 2013). Sanger sequencing was used to confirm the proper orientation of the constructs within the destination vector and the sequence of *EGFP-hoxb5b*. Transgenic embryos were created by co-injecting wild-type embryos at the one-cell stage with 25 pg *hsp70l:EGFP-hoxb5b* vector and 25 pg of *Tol2* mRNA (Kawakami, 2004; Kawakami et al., 2004). Embryos were raised to adulthood and screened for the present of dsRed in the lens at ~3 days and the ability to induce robust EGFP expression following heat-shock (Supplementary Figure S2). Multiple founders for the Tg (*hsp70l:EGFP-hoxb5b;acry:dsRed*)^{ci1014} line were identified so the line that induced the most robust expression following

heat-shock was retained. While some ectopic notochord expression was observed in non-heat shocked embryos they did not exhibit overt phenotypes and developed normally. For heat shock experiments, through routine outcrossing of transgenic animals to the wild type embryos of the AB/TL backgrounds, GFP-*hoxb5b*^{-/-} siblings are produced with each subsequent breeding, which were heat shocked and processed in parallel.

Preparation and Injections of *hoxb5b* mRNA

Capped *vp16-hoxb5b* mRNA was prepared off a Not1 linearized pCS2+ plasmid containing the *vp16-hoxb5b* coding sequence using the Sp6 mMessage Kit (Ambion), as first reported in (Waxman et al., 2008). The *vp16-hoxb5b* construct encodes for a hyperactive form of Hoxb5b and allowed for lower doses of mRNA to be delivered (Waxman and Yelon, 2009). Embryos were injected prior to the four-cell stage with either 15 pg or 30 pg of mRNA and were empirically determined to produce similar phenotypes. Dosage of mRNA was determined per experimental condition. Uninjected wild type sibling embryos were cultured in parallel with injected animals and used for controls. Dead and grossly malformed embryos were removed from analysis.

In Situ Hybridization

In situ hybridizations were performed similarly to the protocol of Jowett and Lettice, 1994, which should be referenced for specific details. Briefly, antisense digoxigenin-labeled riboprobes were generated from previously characterized plasmids containing sequences for *crestin* (Luo et al., 2001), *foxd3* (Odenthal and Nüsslein-Volhard, 1998; Hochgreb-Hagele and Bronner, 2013), *phox2bb* (Uribe and Bronner, 2015), and *hoxb5b* (Waxman et al., 2008). As per the protocol, PFA-fixed whole mount embryos stored in methanol were rehydrated in PBST, permeabilized with Proteinase K digestion (10 µg/ml), and post-fixed in 4% PFA. Embryos were incubated in probes overnight (~16 h) at 65°C and washed sequentially in graded SSCT buffers. Riboprobes solutions were recovered and stored at -20°C for reuse, with multiple uses leading to minimal loss of signal. Probed embryos were blocked for 1–2 h at ambient temperature in 5% Goat sera in PBST before detection overnight (~16 h) at 4°C using an anti-Digoxigenin-Fab fragments conjugated to Alkaline Phosphatase enzymes (1:1,000 dilution, Roche) in 5% Goat Sera in PBST. Finally, riboprobes were visualized with NBT/BCIP solution (3.5 µL each of NBT, BCIP stock solutions, Roche). Probes were validated prior to use on wildtype embryos to calibrate staining duration, with patterns compared to those curated on ZFIN (Howe et al., 2013; Ruzicka et al., 2019).

Whole Mount Immunohistochemistry, HCR, and WICHCR

Immunohistochemistry (IHC), Hybridization Chain Reaction (HCR), and Whole mount Immuno-Coupled Hybridization Chain Reaction (WICHCR) protocols all were conducted according to the methods published in Ibarra-García-Padilla et al., 2021. All IHC assays conducted in blocking 5% Goat Sera in 1X PBST. Primary antibodies against the following

TABLE 1 | Summary of Statistical Tests.

Figure	Panel	Condition	Age	Comparison to Control	Test	p-value	Control Animal N	Experimental Animal N
2	E	norm area POD Crestin + stain	32 hpf	vp16-hoxb5b	T-test	7.75E-07	27	21
2	E	norm area POD Crestin + stain	50 hpf	vp16-hoxb5b	T-test	1.14E-03	7	8
3	E	norm area POD foxd3 + stain	32 hpf	vp16-hoxb5b	Welch's T-test	5.71E-03	7	10
3	F	norm area hindbrain Phox2bb + stain	32 hpf	vp16-hoxb5b	Welch's T-test	0.01	7	8
3	G	norm area POD phox2bb + stain	32 hpf	vp16-hoxb5b	Welch's T-test	5.63E-03	7	8
3	O	POD phox2b + cells	32 hpf	15 pg vp16-hoxb5b	T-test	3.03E-05	7	9
3	O	POD phox2b + cells	32 hpf	30 pg vp16-hoxb5b	T-test	2.61E-05	7	5
4	I	norm area POD Crestin + stain	HS 14 24 hpf	hsp70:GFP-hoxb5b+	T-test	0.02	6	8
4	J	norm area POD Crestin + stain	HS 22 26-28 hpf	hsp70:GFP-hoxb5b+	T-test	0.04	10	14
5	E	# total Enteric Phox2b + cells	50 hpf	15 pg vp16-hoxb5b	T-test	1.83E-04	10	7
5	E	# total Enteric Phox2b + cells	50 hpf	30 pg vp16-hoxb5b	Welch's T-test	3.01E-04	10	9
5	F	# POD phox2b + cells	50 hpf	15 pg vp16-hoxb5b	Wilcoxon Test	3.28E-03	10	7
5	F	# POD phox2b + cells	50 hpf	30 pg vp16-hoxb5b	Kruskal-Wallis Test	6.80E-04	10	9
5	J	# Total Kaede + cells	3 dpf	15 pg vp16-hoxb5b	T-test	1.10E-04	7	8
5	J	# Total Kaede + cells	3 dpf	30 pg vp16-hoxb5b	T-test	4.09E-05	7	7
5	K	# Total Elavl3/4 + cells	3 dpf	15 pg vp16-hoxb5b	T-test	1.35E-03	7	8
5	K	# Total Elavl3/4 + cells	3 dpf	30 pg vp16-hoxb5b	T-test	1.04E-04	7	7
5	L	Copositive Elavl3/4+/Kaede + cells of Total Kaede + cells	3 dpf	15 pg vp16-hoxb5b	Wilcoxon Test	0.13	7	8
5	L	Copositive Elavl3/4 +/-Kaede+ cells of Total Kaede + cells	3 dpf	30 pg vp16-hoxb5b	T-test	0.10	7	7
5S	I	# Gut Restricted Phox2b + Cells	50 hpf	15 pg vp16-hoxb5b	T-test	5.68E-04	10	7
5S	I	# Gut Restricted Phox2b + Cells	50 hpf	30 pg vp16-hoxb5b	Welch's T-test	3.98E-04	10	9
5S	J	Cell Fraction, POD Localized	50 hpf	15 pg vp16-hoxb5b	T-test	0.25	10	7
5S	J	Cell Fraction, POD Localized	50 hpf	30 pg vp16-hoxb5b	T-test	0.37	10	9
5S	J	Cell Fraction, Gut Localized	50 hpf	15 pg vp16-hoxb5b	T-test	0.25	10	7
5S	J	Cell Fraction, Gut Localized	50 hpf	30 pg vp16-hoxb5b	T-test	0.35	10	9
6	H	elavl3/4+ cells	HS 14 3 dpf	hsp70:GFP-hoxb5b+	T-test	2.32E-04	6	11
6	H	elavl3/4 + cells	HS 21 3 dpf	hsp70:GFP-hoxb5b+	T-test	1.68E-03	6	10
6	H	elavl3/4 + cells	HS 48 3 dpf	hsp70:GFP-hoxb5b+	T-test	0.58	12	14
7	C	# GFP + cells	63 hpf	Enteric GFP+	T-test	0.26	6	6
7	C	# Phox2b + cells	63 hpf	Enteric Phox2b+	T-test	0.79	6	6
7	D	Fraction Phox2b + copositive sox10:GFP cells	63 hpf	15 pg vp16-hoxb5b	T-test	0.13	6	6

proteins were used as follows: Phox2b (1:200, Santa Cruz, B-11), Kaede (1:500, MBL International, PM102M), Elavl3/4 (Same as HuC/D, 1:500, Invitrogen Molecular Probes, A21271), Activated Caspase-3 (1:200, BD Biosciences, 559565). Incubation in primary antibody solutions were conducted overnight at 4°C, except for assays with Phox2b or Caspase-3 antibodies which were allowed to incubate for 2 days at 4°C which provided optimal labeling. Corresponding secondary antibodies conjugated to spectrally distinct fluorophores were all used at 1:500 dilution, selected from the following depending on the experimental condition: Alexa Fluor 488 goat anti-rabbit IgG (ThermoFischer, A11008), Alexa Fluor 568 goat anti-rabbit IgG (ThermoFischer, A11011), Alexa Fluor 488 goat anti-mouse IgG1 (ThermoFischer, A21121), Alexa Fluor 594 goat anti-mouse IgG1 (ThermoFischer, A21125), Alexa Fluor 647 goat anti-mouse IgG1 (ThermoFischer, A21240), and Alexa Fluor 647 goat anti-mouse IgG2b (ThermoFischer, A21242). In the HCR and WICHCR assays, commercially designed probes were secured from Molecular Instruments as follows: *crestin* (B3, AF195881.1), *hoxb5b* (B2, BC078285.1), *phox2bb* (B1, NM_001014818.1), and used as prior (Ibarra-García-Padilla et al., 2021). Corresponding amplifiers were purchased from Molecular instruments and were used in experiments to include spectrally distinct fluorophores suitable for multiplexed imaging.

Heat Shock Induction of the *hsp70l: GFP-hoxb5b* Transgene

Adult zebrafish maintained as an outcross and positive for dsRed expression as larvae in the lens (see above method on description of the line) were bred to produce synchronously staged embryos. At the stage designated to begin the heat shock, embryos were rapidly transferred to 37°C E3 and maintained at that temperature. After a 1-h incubation, embryos were rapidly returned to 28°C. In the 1–3 h after heat shock GFP-Hoxb5b⁺ embryos were sorted from GFP⁻ siblings and cultured in parallel until the designated stage for tissue collection.

Imaging, Quantification, and Image Visualization

All embryos prior to imaging were cleared through graded washes of PBST/Glycerol to reach a final Glycerol content of 75%. Fluorescent Z-stacked images of IHC processed embryos were captured using an Olympus FV3000 point scanning confocal microscope supported by Fluoview Acquisition Software (version FV31S-SW). Images were stitched in FIJI (ImageJ version 1.53e) using the Grid/Collection applet as part of the Stitching plugin (Schindelin et al., 2012; Schneider et al., 2012; Rueden et al., 2017). Digital image files were converted with ImarisFileConverter Software (Bitplane) to three dimensional rendered images compatible with IMARIS (V9.4, V9.7, Bitplane). All images of fluorescent animals represented in this publication are derived from maximum intensity projections of the z-stacked image. Cells counts were conducted on volume images following an arithmetic background subtraction in IMARIS to ensure accurate counts, particularly when

determining coincidence of labels. ISH processed embryos were imaged on a Nikon Eclipse Ni microscope equipped with a motorized stage. Z-stack images were acquired and extended depth of focus images were generated in the Nikon NIS-Elements BR software (v5.02.00). Areas of expression were measured in FIJI to include dark pixels in the post-otic or hindbrain domains. Quantifications were curated and analyzed in the Rstudio programming environment (v1.1.463). Images of pigmented embryos were captured similarly on the Nikon microscope with lateral illumination to distinguish iridophores, similar to (Petratou et al., 2021).

In vivo Confocal Microscopy

Embryos were sorted for RFP expression, anesthetized with 0.4% tricaine, and embedded in 1% low melting agarose in a 28.5°C chamber with a coverslip glass bottom. Care was taken to ensure embryo angled appropriately and proximal to the glass. Z-stack images were acquired approximately every half hour concurrently on the same Olympus FV3000 point scanning confocal microscope as above. Maximum intensity projections images were generated and exported from FIJI.

Statistical Analysis

An α of 0.05 was used as a cut off for all statistical tests. Normalcy of datasets was assessed by visual inspection of a density plot, a qqplot against a linear theoretical distribution, and Shapiro-Wilk test for Normalcy. Further, variance between each dataset was examined either with a Bartlett test for data which adhered to normalcy or with a Levene's test for non-normal data. Based on the normalcy and scedasticity conditions of the data, the appropriate statistical test was selected, as summarized in **Table 1**. All statistical analyses were carried out in the Rstudio (v1.1.463) programming environment, with key dependencies on the lawstat (v3.4) and stats (v3.6.3) packages. Plots were generated in Rstudio supported by the ggplot2 (v3.3.2) and ggsignif (v0.6.0) packages.

DATA AVAILABILITY STATEMENT

The original contributions presented in the study are included in the article/**Supplementary Material**, further inquiries can be directed to the corresponding author.

ETHICS STATEMENT

The animal study was reviewed and approved by the Institutional Animal Care and Use Committee (IACUC) of Rice University and Cincinnati Children's Hospital Medical Center.

AUTHOR CONTRIBUTIONS

AH and RU designed the experiments and wrote the manuscript. RU and AA conceived the idea. AH, AN, JT, PR, ES, CL, GK, and RU performed the experiments. PR and JW created the zebrafish transgenic line. AH and RU performed the data analyses. All the

authors contributed to the article and approved the submitted version.

FUNDING

This work was supported by Rice University, a Burroughs Wellcome Fund PDEP Award, Cancer Prevention and Research Institute of Texas (CPRIT) Recruitment of First-Time Tenure Track Faculty Members (No. CPRIT-RR170062) and the NSF CAREER Award (No. 1942019) awarded to RU as well as through the NIH NHLBI (Nos. HL137766, HL141186) awarded to JW.

ACKNOWLEDGMENTS

We offer our sincerest gratitude to Dr. Dan Wagner and to the entire Uribe Lab at Rice University for their insights and support throughout this project. We thank Dr. Budi Utama and the Rice University Shared Equipment Authority on IMARIS image analysis suite, which was indispensable toward this project. We thank Dr. Eric Bridenbaugh and Dr. Mariane Martinez at Olympus for their expert advice on confocal microscopy. We also thank Jonny Diaz and A. Augello Cook for technical assistance.

SUPPLEMENTARY MATERIAL

The Supplementary Material for this article can be found online at: <https://www.frontiersin.org/articles/10.3389/fcell.2021.803370/full#supplementary-material>

Supplementary Figure S1 | Phox2b antibody labeling is synonymous with mRNA and transgenic labeling methods. **(A)** 3 dpf *-8.3phox2bb:kaede* larva co-labeled with WICHCR protocol (Ibarra-García-Padilla et al., 2021) showing Kaede labeled cells (green), *phox2bb* mRNA (magenta), and Phox2b protein (cyan). **(B)** Inset images in

the hindbrain exhibit coincidence of all three probes along the Hindbrain (Hb), Pharyngeal (Pa), and PODs (arrowheads). Kaede⁺ cells which are negative for both mRNA and protein are detected at the dorsal most aspect of the motor neuron complex (star) as well as in anterior regions of the presumptive CNS. **(C)** Images highlighting the midgut axis reveals a perfect coincidence of all three enteric labels with very little background, demonstrating the efficacy of the Phox2b antibody as an enteric neural crest label. While nearly every cell is coincident, selected cells are annotated to aid in comparison (arrowheads). Scale bar A: 100 μ m.

Supplementary Figure S2 | Characterization of novel *hsp70l:GFP-hoxb5b* transgenic zebrafish line. **(A)** GFP-Hoxb5b⁺ overexpressing embryos at 24 hpf are easily distinguishable from GFP⁻ siblings 1 hour after heat shock. GFP⁻ and GFP⁺ embryos are cultured and assayed under identical conditions to control for variations induced by growth at an elevated temperature. **(B–C)** GFP-Hoxb5b construct is localized to cell nuclei following heat shock and persists at least a day after initial induction **(C)**. Scale bar B: 100 μ m.

Supplementary Figure S3 | Depletion of NCC-derived cells in the gut is not the result of cell death. **(A–H)** Wholemount IHC embryos stained with an antibody against activated Caspase-3, a marker for apoptotic cells. NCCs are visualized either in the *sox10:GFP* or WT backgrounds in either uninjected or 15 pg *vp16-hoxb5b* injected embryos. Caspase-3⁺ cells are very rare along the length of the vagal domain in all control embryos ranging from 33 hpf to 66 hpf (A,C,E,G). While discrete pockets of Caspase-3⁺ cells are detected proximal to the POD NCC niche at 33 hpf **(B)** and 55 hpf **(D)**, very few co-positive cells are present at these time frames. Later in development at 63–66 hpf **(F,H)** almost no Caspase-3⁺ cells remain along the posterior aspect of the embryo, with only ectopic labeling of the somatic myotome detectable.

Supplementary Figure S4 | Vagal NCC derivatives following Hoxb5b overexpression are largely unaffected. **(A–D)** Investigation of distinct NCC derived pigment lineages, melanophores (red arrowheads) and iridophores (yellow arrowheads), in 5 dpf embryos overexpressing Hoxb5b compared to controls. **(E,F)** Both control embryos and Hoxb5b overexpressing embryos by 50 hpf produced phenotypically wild type anterior dorsal root ganglia (DRG), as shown in whole mount immunolabeling with an antibody against Elav3/4. **(G,H)** Position and development of the Superior Cervical Ganglion (SCG) occurs by the third day, as shown by immuno labeling for Elav3/4 (red arrowhead). **(I)** Quantifications from animals in **Figure 5**, showing the number of Phox2b⁺ cells localized along the gut length, excluding the POD increases in response to *vp16-hoxb5b* mRNA induction (I, 15 pg: $p = 9.92 \times 10^{-6}$; 30 pg: $p = 0.000404$). **(J)** The distribution of Phox2b⁺ cells between the POD and the length of the gut was unchanged following elevated Hoxb5b activity **(J)**, 15 pg in POD: $p = 0.2515$; 30 pg in POD: $p = 0.3673$; 15 pg in Gut: $p = 0.2306$; 30 pg in Gut: $p = 0.3496$. Scale Bars **(E,F,G,H)**: 50 μ m.

REFERENCES

- Amores, A., Force, A., Yan, Y. L., Joly, L., Amemiya, C., Fritz, A., et al. (1998). Zebrafish Hox Clusters and Vertebrate Genome Evolution. *Science* 282, 1711–1714. doi:10.1126/science.282.5394.1711
- Barsh, G. R., Isabella, A. J., and Moens, C. B. (2017). Vagus Motor Neuron Topographic Map Determined by Parallel Mechanisms of Hox5 Expression and Time of Axon Initiation. *Curr. Biol.* 27, 3812–3825. doi:10.1016/j.cub.2017.11.022
- Breau, M. A., Wilkinson, D. G., and Xu, Q. (2013). A Hox Gene Controls Lateral Line Cell Migration by Regulating Chemokine Receptor Expression Downstream of Wnt Signaling. *Proc. Natl. Acad. Sci.* 110, 16892–16897. doi:10.1073/pnas.1306282110
- Carney, T. J., Dutton, K. A., Greenhill, E., Delfino-Machin, M., Dufourcq, P., Blader, P., et al. (2006). A Direct Role for Sox10 in Specification of Neural Crest-Derived Sensory Neurons. *Development* 133, 4619–4630. doi:10.1242/dev.02668
- Choi, H. M. T., Schwarzkopf, M., Fornace, M. E., Acharya, A., Artavanis, G., Stegmaier, J., et al. (2018). Third-generation *In Situ* Hybridization Chain Reaction: Multiplexed, Quantitative, Sensitive, Versatile, Robust. *Development* 145, dev165753. doi:10.1242/dev.165753
- Choi, H. M. T., Calvert, C. R., Husain, N., Huss, D., Barsi, J. C., Deverman, B. E., et al. (2016). Mapping a Multiplexed Zoo of mRNA Expression. *Development* 143, 3632–3637. doi:10.1242/dev.140137
- Choi, H. M. T., Chang, J. Y., Trinh, L. A., Padilla, J. E., Fraser, S. E., and Pierce, N. A. (2010). Programmable *In Situ* Amplification for Multiplexed Imaging of mRNA Expression. *Nat. Biotechnol.* 28, 1208–1212. doi:10.1038/nbt.1692
- Condie, B. G., and Capecchi, M. R. (1993). Mice Homozygous for a Targeted Disruption of Hoxd-3 (Hox-4.1) Exhibit Anterior Transformations of the First and Second Cervical Vertebrae, the Atlas and the axis. *Development* 119, 579–595. doi:10.1242/dev.119.3.579
- Condie, B. G., and Capecchi, M. R. (1994). Mice with Targeted Disruptions in the Paralogous Genes Hoxa-3 and Hoxd-3 Reveal Synergistic Interactions. *Nature* 370, 304–307. doi:10.1038/370304a0
- Creuzet, S., Couly, G., Vincent, C., and Le Douarin, N. M. (2002). Negative Effect of Hox Gene Expression on the Development of the Neural Crest-Derived Facial Skeleton. *Development* 129, 4301–4313. doi:10.1242/dev.129.18.4301
- Dalgin, G., and Prince, V. E. (2021). Midline Morphogenesis of Zebrafish Foregut Endoderm Is Dependent on Hoxb5b. *Developmental Biol.* 471, 1–9. doi:10.1016/j.ydbio.2020.12.001
- Di Bonito, M., Glover, J. C., and Studer, M. (2013). Hoxgenes and Region-specific Sensorimotor Circuit Formation in the Hindbrain and Spinal Cord. *Dev. Dyn.* 242, 1348–1368. doi:10.1002/dvdy.24055
- Di Giacomio, G., Koss, M., Capellini, T. D., Brendolan, A., Pöpperl, H., and Selleri, L. (2006). Spatio-temporal Expression of Pbx3 during Mouse Organogenesis. *Gene Expr. Patterns* 6, 747–757. doi:10.1016/j.modgep.2005.12.002
- Durbec, P. L., Larsson-blomberg, L. B., Schuchardt, A., Costantini, F., and Pachnis, V. (1996). Common Origin and Developmental Dependence on C-Ret of

- Subsets of Enteric and Sympathetic Neuroblasts. *Development* 122, 349–358. doi:10.1242/dev.122.1.349
- Elworthy, S., Pinto, J. P., Pettifer, A., Cancela, M. L., and Kelsh, R. N. (2005). Phox2b Function in the Enteric Nervous System Is Conserved in Zebrafish and Is Sox10-dependent. *Mech. Development* 122, 659–669. doi:10.1016/j.mod.2004.12.008
- Ganz, J. (2018). Gut Feelings: Studying Enteric Nervous System Development, Function, and Disease in the Zebrafish Model System. *Dev. Dyn.* 247, 268–278. doi:10.1002/dvdy.24597
- Gouti, M., Briscoe, J., and Gavalas, A. (2011). Anterior Hox Genes Interact with Components of the Neural Crest Specification Network to Induce Neural Crest Fates. *Stem Cells* 29, 858–870. doi:10.1002/stem.630
- Harrison, C., Wabbersen, T., and Shepherd, I. T. (2014). *In Vivo* visualization of the Development of the Enteric Nervous System Using aTg(-8.3bphox2b:Kaede) transgenic Zebrafish. *Genesis* 52, 985–990. doi:10.1002/dvg.22826
- Hochgreb-Hägele, T., and Bronner, M. E. (2013). A Novel FoxD3 Gene Trap Line Reveals Neural Crest Precursor Movement and a Role for FoxD3 in Their Specification. *Developmental Biol.* 374, 1–11. doi:10.1016/j.ydbio.2012.11.035
- Hortopan, G. A., and Baraban, S. C. (2011). Aberrant Expression of Genes Necessary for Neuronal Development and Notch Signaling in an Epileptic Mind Bomb Zebrafish. *Dev. Dyn.* 240, 1964–1976. doi:10.1002/dvdy.22680
- Howard, A. G. A., Baker, P. A., Ibarra-García-Padilla, R., Moore, J. A., Rivas, L. J., Tallman, J. J., et al. (2021). An Atlas of Neural Crest Lineages along the Posterior Developing Zebrafish at Single-Cell Resolution. *Elife* 10, e60005. doi:10.7554/elife.60005
- Howe, D. G., Bradford, Y. M., Conlin, T., Eagle, A. E., Fashena, D., Frazer, K., et al. (2013). ZFIN, the Zebrafish Model Organism Database: Increased Support for Mutants and Transgenics. *Nucleic Acids Res.* 41, D854–D860. doi:10.1093/nar/gks938
- Hutchins, E. J., Kunttas, E., Piacentino, M. L., Howard, A. G. A., Bronner, M. E., and Uribe, R. A. (2018). Migration and Diversification of the Vagal Neural Crest. *Dev. Biol.* 444 Suppl 1, S98–S30269. doi:10.1016/j.ydbio.2018.07.004
- Ibarra-García-Padilla, R., Howard, A. G. A., Singleton, E. W., and Uribe, R. A. (2021). A Protocol for Whole-Mount Immuno-Coupled Hybridization Chain Reaction (WICHCR) in Zebrafish Embryos and Larvae. *STAR Protoc.* 2, 100709. doi:10.1016/j.xpro.2021.100709
- Jarinova, O., Hatch, G., Poitras, L., Prudhomme, C., Grzyb, M., Aubin, J., et al. (2008). Functional Resolution of Duplicatedhoxb5genes in Teleosts. *Development* 135, 3543–3553. doi:10.1242/dev.025817
- Jowett, T., and Lettice, L. (1994). Whole-mount *In Situ* Hybridization on Zebrafish Embryos Using a Mixture of Digoxigenin- and Fluorescein-Labeled Probes. *Trends Genet.* 10, 73–74. doi:10.1016/0168-9525(94)90220-8
- Kam, M. K. M., Cheung, M. C. H., Zhu, J. J., Cheng, W. W. C., Sat, E. W. Y., Tam, P. K. H., et al. (2014b). Perturbation of Hoxb5 Signaling in Vagal and Trunk Neural Crest Cells Causes Apoptosis and Neurocristopathies in Mice. *Cell Death Differ.* 21, 278–289. doi:10.1038/cdd.2013.142
- Kam, M. K. M., Cheung, M., Zhu, J. J., Cheng, W. W. C., Sat, E. W. Y., Tam, P. K. H., et al. (2014a). Homeobox B5 (Hoxb5) Regulates the Expression of Forkhead Box D3 Gene (Foxd3) in Neural Crest. *Int. J. Biochem. Cell Biol.* 55, 144–152. doi:10.1016/j.biocel.2014.09.002
- Kam, M. K. M., and Lui, V. C. H. (2015). Roles of Hoxb5 in the Development of Vagal and Trunk Neural Crest Cells. *Develop. Growth Differ.* 57, 158–168. doi:10.1111/dgd.12199
- Karlsson, J., Von Hofsten, J., and Olsson, P. E. (2001). Generating Transparent Zebrafish: A Refined Method to Improve Detection of Gene Expression during Embryonic Development. *Mar. Biotechnol. (Ny)* 3, 522–527. doi:10.1007/s1012601-0053-4
- Kawakami, K., Takeda, H., Kawakami, N., Kobayashi, M., Matsuda, N., and Mishina, M. (2004). A Transposon-Mediated Gene Trap Approach Identifies Developmentally Regulated Genes in Zebrafish. *Developmental Cell.* 7, 133–144. doi:10.1016/j.devcel.2004.06.005
- Kawakami, K. (2004). “Transgenesis and Gene Trap Methods in Zebrafish by Using the Tol2 Transposable Element,” in *Methods in Cell Biology* (Academic Press), 201–222. doi:10.1016/s0091-679x(04)77011-9
- Kucenas, S., Takada, N., Park, H.-C., Woodruff, E., Broadie, K., and Appel, B. (2008). CNS-derived Glia Ensheath Peripheral Nerves and Mediate Motor Root Development. *Nat. Neurosci.* 11, 143–151. doi:10.1038/nn2025
- Kudoh, T., Tsang, M., Hukriede, N. A., Chen, X., Dedekian, M., Clarke, C. J., et al. (2001). A Gene Expression Screen in Zebrafish Embryogenesis. *Genome Res.* 11, 1979–1987. doi:10.1101/gr.209601
- Kwan, K. M., Fujimoto, E., Grabher, C., Mangum, B. D., Hardy, M. E., Campbell, D. S., et al. (2007). The Tol2kit: A Multisite Gateway-Based Construction Kit for Tol2 Transposon Transgenesis Constructs. *Dev. Dyn.* 236, 3088–3099. doi:10.1002/dvdy.21343
- Le Douarin, N., and Kalcheim, C. (1999). *The Neural Crest*. Cambridge University Press.
- Le Douarin, N. M. (1982). *The Neural Crest*. Cambridge: Cambridge University Press.
- Lengerke, C., Schmitt, S., Bowman, T. V., Jang, I. H., Maouche-Chretien, L., McKinney-Freeman, S., et al. (2008). BMP and Wnt Specify Hematopoietic Fate by Activation of the Cdx-Hox Pathway. *Cell Stem Cell* 2, 72–82. doi:10.1016/j.stem.2007.10.022
- Lister, J. A., Cooper, C., Nguyen, K., Modrell, M., Grant, K., and Raible, D. W. (2006). Zebrafish Foxd3 Is Required for Development of a Subset of Neural Crest Derivatives. *Developmental Biol.* 290, 92–104. doi:10.1016/j.ydbio.2005.11.014
- Lui, V. C. H., Cheng, W. W. C., Leon, T. Y. Y., Lau, D. K. C., Garcia-Bareclo, M. M., Miao, X. P., et al. (2008). Perturbation of Hoxb5 Signaling in Vagal Neural Crests Down-Regulates Ret Leading to Intestinal Hypoganglionosis in Mice. *Gastroenterology* 134, 1104–1115. doi:10.1053/j.gastro.2008.01.028
- Luo, R., An, M., Arduini, B. L., and Henion, P. D. (2001). Specific Pan-Neural Crest Expression of zebrafishCrestin throughout Embryonic Development. *Dev. Dyn.* 220, 169–174. doi:10.1002/1097-0177(2000)9999:9999<aid-dvdy1097>3.0.co;2-1
- Mandal, A., Rydeen, A., Anderson, J., Sorrell, M. R. J., Zygmont, T., Torres-Vázquez, J., et al. (2013). Transgenic Retinoic Acid Sensor Lines in Zebrafish Indicate Regions of Available Embryonic Retinoic Acid. *Dev. Dyn.* 242, 989–1000. doi:10.1002/dvdy.23987
- Martik, M. L., and Bronner, M. E. (2017). Regulatory Logic Underlying Diversification of the Neural Crest. *Trends Genet.* 33, 715–727. doi:10.1016/j.tig.2017.07.015
- Minguillon, C., Nishimoto, S., Wood, S., Vendrell, E., Gibson-Brown, J. J., and Logan, M. P. O. (2012). Hox Genes Regulate the Onset of Tbx5 Expression in the Forelimb. *Development* 139, 3180–3188. doi:10.1242/dev.084814
- Nagy, N., and Goldstein, A. M. (2017). Enteric Nervous System Development: A Crest Cell’s Journey from Neural Tube to colon. *Semin. Cell Developmental Biol.* 66, 94–106. doi:10.1016/j.semdev.2017.01.006
- Odenthal, J., and Nüsslein-Volhard, C. (1998). fork Head Domain Genes in Zebrafish. *Development Genes Evol.* 208, 245–258. doi:10.1007/s004270050179
- Parker, H. J., De Kumar, B., Green, S. A., Prummel, K. D., Hess, C., Kaufman, C. K., et al. (2019). A Hox-TALE Regulatory Circuit for Neural Crest Patterning Is Conserved across Vertebrates. *Nat. Commun.* 10, 1189. doi:10.1038/s41467-019-09197-8
- Parker, H. J., Pushel, I., and Krumlauf, R. (2018). Coupling the Roles of Hox Genes to Regulatory Networks Patterning Cranial Neural Crest. *Developmental Biol.* 444, S67–S78. doi:10.1016/j.ydbio.2018.03.016
- Pattyn, A., Morin, X., Cremer, H., Goridis, C., and Brunet, J.-F. (1999). The Homeobox Gene Phox2b Is Essential for the Development of Autonomic Neural Crest Derivatives. *Nature* 399, 366–370. doi:10.1038/20700
- Pearson, J. C., Lemons, D., and McGinnis, W. (2005). Modulating Hox Gene Functions during Animal Body Patterning. *Nat. Rev. Genet.* 6, 893–904. doi:10.1038/nrg1726
- Petratou, K., Spencer, S. A., Kelsh, R. N., and Lister, J. A. (2021). The MITF Paralog Tfec Is Required in Neural Crest Development for Fate Specification of the Iridophore Lineage from a Multipotent Pigment Cell Progenitor. *PLoS One* 16, e0244794. doi:10.1371/journal.pone.0244794
- Rancourt, D. E., Tsuzuki, T., and Capecchi, M. R. (1995). Genetic Interaction between Hoxb-5 and Hoxb-6 Is Revealed by Nonallelic Noncomplementation. *Genes Dev.* 9, 108–122. doi:10.1101/gad.9.1.108
- Rocha, M., Singh, N., Ahsan, K., Beiriger, A., and Prince, V. E. (2020). Neural Crest Development: Insights from the Zebrafish. *Developmental Dyn.* 249, 88–111. doi:10.1002/dvdy.122
- Rueden, C. T., Schindelin, J., Hiner, M. C., DeZonia, B. E., Walter, A. E., Arena, E. T., et al. (2017). ImageJ2: ImageJ for the Next Generation of Scientific Image Data. *BMC Bioinformatics* 18, 529. doi:10.1186/s12859-017-1934-z

- Ruzicka, L., Howe, D. G., Ramachandran, S., Toro, S., Van Slyke, C. E., Bradford, Y. M., et al. (2019). The Zebrafish Information Network: New Support for Non-coding Genes, Richer Gene Ontology Annotations and the Alliance of Genome Resources. *Nucleic Acids Res.* 47, D867–D873. doi:10.1093/nar/gky1090
- Santini, S., Boore, J. L., and Meyer, A. (2003). Evolutionary Conservation of Regulatory Elements in Vertebrate Hox Gene Clusters. *Genome Res.* 13, 1111–1122. doi:10.1101/gr.700503
- Schindelin, J., Arganda-Carreras, I., Frise, E., Kaynig, V., Longair, M., Pietzsch, T., et al. (2012). Fiji: an Open-Source Platform for Biological-Image Analysis. *Nat. Methods* 9, 676–682. doi:10.1038/nmeth.2019
- Schneider, C. A., Rasband, W. S., and Eliceiri, K. W. (2012). NIH Image to ImageJ: 25 Years of Image Analysis. *Nat. Methods* 9, 671–675. doi:10.1038/nmeth.2089
- Simoes-Costa, M., and Bronner, M. E. (2016). Reprogramming of Avian Neural Crest Axial Identity and Cell Fate. *Science* 352, 1570–1573. doi:10.1126/science.aaf2729
- Soldatov, R., Kaucka, M., Kastriti, M. E., Petersen, J., Chontorotzea, T., Englmaier, L., et al. (2019). Spatiotemporal Structure of Cell Fate Decisions in Murine Neural Crest. *Science* 364, eaas9536. doi:10.1126/science.aas9536
- Sorrells, S., Toruno, C., Stewart, R. A., and Jette, C. (2013). Analysis of Apoptosis in Zebrafish Embryos by Whole-Mount Immunofluorescence to Detect Activated Caspase 3. *JoVE* 82, 51060. doi:10.3791/51060
- Tang, W., Li, Y., Li, A., and Bronner, M. E. (2021). Clonal Analysis and Dynamic Imaging Identify Multipotency of Individual Gallus gallus Caudal Hindbrain Neural Crest Cells toward Cardiac and Enteric Fates. *Nat. Commun.* 12, 1894. doi:10.1038/s41467-021-22146-8
- Tennyson, V. M., Gershon, M. D., Sherman, D. L., Behringer, R. R., Raz, R., Crotty, D. A., et al. (1993). Structural Abnormalities Associated with Congenital Megacolon in Transgenic Mice that Overexpress the Hoxa-4 Gene. *Dev. Dyn.* 198, 28–53. doi:10.1002/aja.1001980105
- Uribe, R. A., and Bronner, M. E. (2015). Meis3 Is Required for Neural Crest Invasion of the Gut during Zebrafish Enteric Nervous System Development. *MBoC* 26, 3728–3740. doi:10.1091/mbc.e15-02-0112
- van der Velden, Y. U., Wang, L., van Lohuizen, M., and Haramis, A.-P. G. (2012). The Polycomb Group Protein Ring1b Is Essential for Pectoral Fin Development. *Development* 139, 2210–2220. doi:10.1242/dev.077156
- Waxman, J. S., Keegan, B. R., Roberts, R. W., Poss, K. D., and Yelon, D. (2008). Hoxb5b Acts Downstream of Retinoic Acid Signaling in the Forelimb Field to Restrict Heart Field Potential in Zebrafish. *Developmental Cel.* 15, 923–934. doi:10.1016/j.devcel.2008.09.009
- Waxman, J. S., and Yelon, D. (2009). Increased Hox Activity Mimics the Teratogenic Effects of Excess Retinoic Acid Signaling. *Dev. Dyn.* 238, 1207–1213. doi:10.1002/dvdy.21951
- Wolgemuth, D. J., Behringer, R. R., Mostoller, M. P., Brinster, R. L., and Palmiter, R. D. (1989). Transgenic Mice Overexpressing the Mouse Homoeobox-Containing Gene Hox-1.4 Exhibit Abnormal Gut Development. *Nature* 337, 464–467. doi:10.1038/337464a0
- Zhu, K., Spaink, H. P., and Durston, A. J. (2017). Collinear Hox-Hox Interactions Are Involved in Patterning the Vertebrate Anteroposterior (A-P) axis. *PLoS One* 12, e0175287–15. doi:10.1371/journal.pone.0175287

Conflict of Interest: The authors declare that the research was conducted in the absence of any commercial or financial relationships that could be construed as a potential conflict of interest.

Publisher's Note: All claims expressed in this article are solely those of the authors and do not necessarily represent those of their affiliated organizations, or those of the publisher, the editors and the reviewers. Any product that may be evaluated in this article, or claim that may be made by its manufacturer, is not guaranteed or endorsed by the publisher.

Copyright © 2022 Howard, Nguyen, Tworig, Ravisankar, Singleton, Li, Kotzur, Waxman and Uribe. This is an open-access article distributed under the terms of the Creative Commons Attribution License (CC BY). The use, distribution or reproduction in other forums is permitted, provided the original author(s) and the copyright owner(s) are credited and that the original publication in this journal is cited, in accordance with accepted academic practice. No use, distribution or reproduction is permitted which does not comply with these terms.